AGU PUBLICATIONS

Journal of Advances in Modeling Earth Systems

RESEARCH ARTICLE
10.1002/2014MS000360

Key Points:
- Comprehensive evaluation of improved CESM with surface/satellite observations
- Comparable or better performance for improved CESM/CAM5 than CESM-CMIP5
- Anthropogenic emissions can have sizeable impacts on radiation and climate

Correspondence to:
Y. Zhang,
yang_zhang@ncsu.edu

Citation:
He, J., Y. Zhang, T. Glotfelty, R. He, R. Bennartz, J. Rausch, and K. Sartelet (2015), Decadal simulation and comprehensive evaluation of CESM/CAM5.1 with advanced chemistry, aerosol microphysics, and aerosol-cloud interactions, *J. Adv. Model. Earth Syst.*, *07*, doi:10.1002/2014MS000360.

Received 5 JUL 2014
Accepted 29 DEC 2014
Accepted article online 19 JAN 2015

Decadal simulation and comprehensive evaluation of CESM/CAM5.1 with advanced chemistry, aerosol microphysics, and aerosol-cloud interactions

Jian He[1], Yang Zhang[1], Tim Glotfelty[1], Ruoying He[1], Ralf Bennartz[2,3], John Rausch[4], and Karine Sartelet[5]

[1]Department of Marine, Earth, and Atmospheric Sciences, North Carolina State University, Raleigh, North Carolina, USA, [2]Department of Earth and Environmental Sciences, Vanderbilt University, Nashville, Tennessee, USA, [3]Department of Space Science and Engineering Center, University of Wisconsin-Madison, Madison, Wisconsin, USA, [4]Department of Atmospheric and Oceanic Sciences, University of Wisconsin-Madison, Madison, Wisconsin, USA, [5]CEREA (Atmospheric Environment Center), Joint Laboratory École des Ponts ParisTech and EDF R&D, Université Paris-Est, Marne-la-Vallée, France

Abstract Earth system models have been used for climate predictions in recent years due to their capabilities to include biogeochemical cycles, human impacts, as well as coupled and interactive representations of Earth system components (e.g., atmosphere, ocean, land, and sea ice). In this work, the Community Earth System Model (CESM) with advanced chemistry and aerosol treatments, referred to as CESM-NCSU, is applied for decadal (2001–2010) global climate predictions. A comprehensive evaluation is performed focusing on the atmospheric component—the Community Atmosphere Model version 5.1 (CAM5.1) by comparing simulation results with observations/reanalysis data and CESM ensemble simulations from the Coupled Model Intercomparison Project phase 5 (CMIP5). The improved model can predict most meteorological and radiative variables relatively well with normalized mean biases (NMBs) of −14.1 to −9.7% and 0.7–10.8%, respectively, although temperature at 2 m (T2) is slightly underpredicted. Cloud variables such as cloud fraction (CF) and precipitating water vapor (PWV) are well predicted, with NMBs of −10.5 to 0.4%, whereas cloud condensation nuclei (CCN), cloud liquid water path (LWP), and cloud optical thickness (COT) are moderately-to-largely underpredicted, with NMBs of −82.2 to −31.2%, and cloud droplet number concentration (CDNC) is overpredictd by 26.7%. These biases indicate the limitations and uncertainties associated with cloud microphysics (e.g., resolved clouds and subgrid-scale cumulus clouds). Chemical concentrations over the continental U.S. (CONUS) (e.g., SO_4^{2-}, Cl^-, OC, and $PM_{2.5}$) are reasonably well predicted with NMBs of −12.8 to −1.18%. Concentrations of SO_2, SO_4^{2-}, and PM_{10} are also reasonably well predicted over Europe with NMBs of −20.8 to −5.2%, so are predictions of SO_2 concentrations over the East Asia with an NMB of −18.2%, and the tropospheric ozone residual (TOR) over the globe with an NMB of −3.5%. Most meteorological and radiative variables predicted by CESM-NCSU agree well overall with those predicted by CESM-CMIP5. The performance of LWP and AOD predicted by CESM-NCSU is better than that of CESM-CMIP5 in terms of model bias and correlation coefficients. Large biases for some chemical predictions can be attributed to uncertainties in the emissions of precursor gases (e.g., SO_2, NH_3, and NO_x) and primary aerosols (black carbon and primary organic matter) as well as uncertainties in formulations of some model components (e.g., online dust and sea-salt emissions, secondary organic aerosol formation, and cloud microphysics). Comparisons of CESM simulation with baseline emissions and 20% of anthropogenic emissions from the baseline emissions indicate that anthropogenic gas and aerosol species can decrease downwelling shortwave radiation (FSDS) by 4.7 W m^{-2} (or by 2.9%) and increase SWCF by 3.2 W m^{-2} (or by 3.1%) in the global mean.

1. Introduction

1.1. Background and Motivation

A number of Earth system models have been developed in recent years to understand climate change and variability by including biogeochemical cycles, human impacts, as well as coupled and interactive representations of Earth system components (e.g., atmosphere, ocean, land, and sea ice). Table 1 summarizes current

Table 1. Atmospheric Component in the Earth System Models

	HadGEM2-ES[a]	GFDL-ESM2[b]	MPI-ESM[c]	MIT-IGSM-CAM[d]	NCAR-CESM[e]	NCSU-CESM[f]
Atmosphere model	HadGEM2-A[g]	AM2[g]	ECHAM6[g]	CAM3[g]	CAM5[g]	CAM5[g]
Gas-phase	*O'Connor et al.* [2014]	Prescribed	Prescribed	Prescribed	(1) Simple chemistry (2) *Emmons et al.* [2010] (3) *Lamarque et al.* [2012]	CB05_GE[i]
Aqueous-phase	SO_2 oxidation by H_2O_2	N.A.[h]	N.A.	N.A.	*Barth et al.* [2000]	*He and Zhang* [2014]
Inorganic aerosol	*Bellouin et al.* [2011]	Prescribed	Prescribed	Prescribed	*Liu et al.* [2012]	*He and Zhang* [2014]
SOA	*Bellouin et al.* [2011]	Prescribed	Prescribed	Prescribed	*Liu et al.* [2012]	*Glotfelty et al.* [2013]
Aerosol activation	N.A.	N.A.	N.A.	N.A.	*Abdul-Razzak and Ghan* [2000]	*Gantt et al.* [2014]
Supported horizontal resolution	1.25° × 1.875°	2° × 2.5°	1.9°	2° × 2.5°	1.9° × 2.5°, 0.9° × 1.25°	0.9° × 1.25°
Supported vertical layers	38	24	47	26	26, 30	30

[a]HadGEM2-ES: the Hadley Centre Global Environmental Model version 2 including Earth system components [*Collins et al.*, 2011].
[b]GFDL-ESM2: the Geophysical Fluid Dynamics Laboratory (GDFL) Earth System Model version 2 [*Dunne et al.*, 2012, 2013].
[c]MPI-ESM: the new Max Planck Institute Earth System Model [*Giorgetta et al.*, 2013].
[d]MIT-IGSM: the Massachusetts Institute of Technology Integrated Global System Model [*Monier et al.*, 2013].
[e]NCAR-CESM: the National Center for Atmospheric Research Community Earth System Model [*Hurrell et al.*, 2013].
[f]NCSU-CESM: the North Carolina State University Community Earth System Model used in this work.
[g]HadGEM2-A: HadGEM2 atmosphere model [*Martin et al.*, 2011]; AM2: the Atmospheric Model version 2 [*GFDL Global Atmospheric Model Development Team*, 2004]; ECHAM6: the sixth generation of atmospheric general circulation developed by the Max Planck Institute for Meteorology [*Stevens et al.*, 2013]; CAM3: Community Atmosphere Model version 3 [*Collins et al.*, 2004]; CAM5: Community Atmosphere Mode version 5 [*Neale et al.*, 2012].
[h]N.A.: not available, it refers to no description about aerosol activation treatment in the model.
[i]CB05_GE: the 2005 Carbon Bond mechanism with global extension [*Karamchandani et al.*, 2012].

Earth system models that are used in the community. The Hadley Centre Global Environmental Model version 2 including Earth system components (HadGEM2-ES) [*Collins et al.*, 2011] developed by U.K. Met Office Hadley Centre is designed for simulating and understanding the centennial-scale evolution of climate including physical, chemical, and biological processes among Earth system components. *Bellouin et al.* [2011] evaluated HadGEM2-ES 1860–2100 simulations in terms of aerosols and discussed the importance of aerosols in the climate system. The Earth System Model version 2 (ESM2) [*Dunne et al.*, 2012, 2013] developed by the Geophysical Fluid Dynamics Laboratory (GDFL) was designed to study carbon-climate interactions and feedbacks within climate systems under the diverse anthropogenic perturbations (e.g., fossil fuel emissions, agriculture and forestry, and aerosol chemistry) within a single self-consistent system. *Dunne et al.* [2012] evaluated the GDFL-ESM2 100 year simulations and discussed the impacts of ocean dynamics on climate variability. The new Max-Planck-Institute Earth System Model (MPI-ESM) [*Giorgetta et al.*, 2013] developed by the Max Planck Institute for Meteorology is designed through diverse model configurations for a series of climate change experiments to estimate climate sensitivity and transient climate change. MPI-ESM simulations through diverse model configurations and experiments associated with different climate forcings have contributed to the Coupled Model Intercomparison Project phase 5 (CMIP5) [*Giorgetta et al.*, 2013]. The Integrated Global System Model (IGSM) [*Dutkiewicz et al.*, 2005; *Sokolov et al.*, 2005] developed by the Massachusetts Institute of Technology (MIT) consists of an economic model, a coupled atmosphere-ocean-land surface model with interactive chemistry, and natural ecosystem models. It is designed to analyze the global environmental changes that may result from anthropogenic causes, quantify the uncertainties associated with the projected changes, and assess the costs and environmental effectiveness of proposed policies to mitigate climate risk. Since IGSM consists of a two-dimensional atmospheric component, *Monier et al.* [2013] coupled IGSM with the Community Atmosphere Model (CAM) developed by the National Center for Atmospheric Research (NCAR) to address regional climate change.

As one of the recent Earth system models, the Community Earth System Model (CESM) [*Hurrell et al.*, 2013] developed by NCAR consists of component models with many capabilities that can be coupled in different configurations for different purposes. These capabilities include interactive carbon-nitrogen cycling, human impacts on vegetation and land use change, a marine ecosystem-biogeochemical module, and new chemical and physical processes to study both the direct and indirect effects of aerosols on climate. CESM can simulate the entire Earth system by coupling the physical climate system with chemistry, biogeochemistry, biology, and human systems. It can also quantify the certainties and uncertainties in Earth system feedbacks on time scales up to centuries and longer. It has been applied to simulate climate change as part of the Intergovernmental Panel on Climate Change (IPCC) Fifth Assessment Report (AR5). However, due to the complexities in physical and chemical processes of aerosols, significant uncertainties remain in the treatments of such processes in the models. For example, many Earth system models do not include chemistry

or use prescribed or highly simplified gas/aerosol treatments in the model simulations. However, gas-phase chemistry and subsequent gas-to-particle conversion processes (e.g., new particle formation, condensation, and thermodynamic partitioning) have large impacts on climate as they influence the amounts and distributions of gaseous precursors and secondary aerosols. Aerosols can influence the Earth's radiative balance by directly scattering and absorbing radiation and indirectly affecting cloud properties through acting as cloud condensation nuclei (CCN) and ice nuclei (IN). Therefore, it is important to accurately simulate aerosol size distribution, chemical composition, and physical and chemical properties, which determine the magnitude of the aerosol radiative forcing [*Koloutsou-Vakakis et al*., 1998]. Uncertainties associated with aerosol-cloud interactions as well as their feedbacks are also among the emerging issues that are to be addressed by the scientific community. To reduce the uncertainties associated with some of those model treatments and the resultant predictions of aerosol impacts on climate, advanced treatments for chemistry and inorganic aerosol [*He and Zhang*, 2014], secondary organic aerosol (SOA) [*Glotfelty et al*., 2013], as well as aerosol activation [*Gantt et al*., 2014] have recently been implemented into the Community Atmosphere Model version 5.1 (CAM5.1), the atmospheric component of CESM version 1.0.5 (CESM1.0.5), by North Carolina State University (NCSU) (referred to as CESM_NCSU in Table 1).

A comprehensive model evaluation must be performed to assess the model's capability to reproduce the current atmosphere before it can be applied to project future climate change. Most Earth system model evaluations have been performed for a single species or component model. For example, *Keppel-Aleks et al*. [2013] evaluated CO_2 variability predicted by CESM. *Lamarque et al*. [2012] evaluated the chemistry model in CESM. *Liu et al*. [2012] and *Ghan et al*. [2012] evaluated the aerosol model and aerosol radiative forcing in CAM5. *Lipscomb et al*. [2013] evaluated the Glimmer Community ICE Sheet model in CESM. *He and Zhang* [2014] implemented advanced gas-phase mechanism and inorganic aerosol treatments into CESM/CAM5 and evaluated the chemistry/aerosol performance from the model simulations with a fully coupled mode and with prescribed SST. *Gantt et al*. [2014] implemented an advanced aerosol activation scheme and evaluated the model performance in simulating aerosol and cloud properties and their impacts on climate using CESM/CAM5 with the advanced aerosol activation scheme. Simulations with each of the updates in the model's representations of chemistry, aerosol, and aerosol-cloud interactions used in this work have been evaluated in *He and Zhang* [2014] and *Gantt et al*. [2014] to illustrate the individual impact of each updated treatment on the overall model predictions. In this work, a comprehensive evaluation of multiple variables and species from CESM/CAM5.1 is conducted through applying the CESM/CAM5.1 with advanced chemistry/aerosol treatments and their interactions with clouds for retrospective decadal simulations during 2001–2010.

The objectives of this work are to comprehensively evaluate the capability of the fully coupled CESM with advanced chemistry/aerosol treatment in reproducing observations (or reanalyses) of climate and air quality variables in 2001–2010, characterize their seasonal and interannual variability, and study interactions among atmospheric chemistry, aerosols, and clouds, as well as their impacts on climate via atmospheric radiation and aerosol direct/indirect effects. Such comprehensive evaluations can provide information to assess the appropriateness of the model for future climate simulations and identify uncertainties/limitations for future model improvement. Through this work, several scientific questions will be addressed. For example, can the improved CESM-CAM5 reproduce the meteorological and chemical observations and their time evolution during a decade-long period? How is its skill for decadal climate modeling compared to the skill of CESM-CMIP5? What are additional uncertainties/limitations in the model treatment for accurate model predictions? (4) What are the contributions of anthropogenic emissions to global radiation and climate for a present-day atmosphere?

2. Model Description

CESM/CAM5.1 used in this work is based on version 1.0.5 that was released by NCAR and further developed and improved at NCSU [*Glotfelty et al*., 2013; *He and Zhang*, 2014; *Gantt et al*., 2014]. The gas-phase chemical mechanism is based on the 2005 Carbon Bond Mechanism for Global Extension (CB05_GE) of *Karamchandani et al*. [2012]. The aerosol module used in the NCSU's version is based on the 7-mode modal aerosol module (MAM7) of CESM/CAM5.1, but with several modifications. First, the new particle formation treatments include a combination of the default nucleation parameterizations of *Vehkamaki et al*. [2002] and

Merikanto et al. [2007], a newly added ion-mediated aerosol nucleation [*Yu*, 2010] above the planetary boundary layer (PBL), and a combination of the three and an additional parameterization of *Wang and Penner* [2009] in the PBL. Second, the inorganic aerosol thermodynamics is based on ISORROPIA II of *Fountoukis and Nenes* [2007] which explicitly simulates the thermodynamics of sulfate (SO_4^{2-}), ammonium (NH_4^+), nitrate (NO_3^-), sodium (Na^+), and chloride (Cl^-) in the Aitken, accumulation, and fine sea-salt modes, as well as the impact of crustal species associated with the fine dust mode. Other updates to the chemistry and aerosol treatments include splitting sea-salt aerosol in MAM7 into sodium and chloride to enable chlorine chemistry in ISORROPIA II, the addition of aqueous-phase dissolution and dissociation of nitric acid (HNO_3) and hydrochloric acid (HCl), and the use of species-dependent accommodation coefficients for sulfuric acid (H_2SO_4), ammonia (NH_3), HNO_3, and HCl, with values of 0.1, 0.097, 0.0024, and 0.005, respectively. For aerosol-cloud interactions, the NCSU version of CESM/CAM5.1 contains an advanced aerosol activation scheme based on *Fountoukis and Nenes* [2005, hereinafter FN05] with additional updates based on *Kumar et al*. [2009, hereinafter K09], *Barahona et al*. [2010, hereinafter B10], and *Gantt et al*. [2014, hereafter referred to as the FN05 series parameterization]. FN05 is based on *Nenes and Seinfeld* [2003] and includes explicit calculations of mass transfer, condensation coefficient, integration over the aerosol size distribution, and kinetic limitations. K09 accounts for insoluble adsorption, which leads to the activation of some particles that would not easily activate under Köhler theory. B10 parameterization accounts for the slow condensation upon internally limited droplets in the calculation of the droplet surface area and maximum supersaturation in a cloud updraft. With all those updates, the advanced aerosol activation scheme accounts for adsorption activation from insoluble CCN and giant CCN equilibrium time scale on aerosol activation. More detailed descriptions of the NCSU version of CESM/CAM5 can be found in *He and Zhang* [2014] and *Gantt et al*. [2014].

In this work, several additional developments and updates have been performed in the NCSU version of CESM/CAM5.1. First, the heterogeneous chemistry has been implemented into CB05 based on *Karamchandani et al*. [2012]; it includes 14 heterogeneous reactions on aerosol particles/cloud droplets and 10 heterogeneous reactions in polar stratospheric clouds (PSCs). Additionally, six kinetic reactions pertaining to the oxidation of anthropogenic and biogenic volatile organic compounds (VOCs) by OH are included in this work; the products of those reactions are linked with the organic gas/aerosol partitioning for SOA formation. Second, a volatility-basis-set (VBS) approach has been implemented into CAM5.1 [*Glotfelty et al*., 2013] to provide an advanced treatment for SOA, which can potentially improve model performance with respect to organic aerosols (OA). VBS provides an empirical representation of the aging and volatility of the OA and its precursors [*Donahue et al*., 2006; *Lane et al*., 2008; *Andreae*, 2009; *Jimenez et al*., 2009; *Ahmadov et al*., 2012]. Using VBS, VOCs are oxidized primarily by OH to form semivolatile organic compounds (SVOCs). The SVOCs partition in both the gas and the condensed phases. The SOA formed from these SVOCs is represented with different volatility bins defined by different effective saturation concentrations. Over time, the SVOCs will be oxidized further and move from the higher volatility bins to the lower volatility bins, where they are more likely to condense to the particulate phase. This approach has been extended to a two-dimensional model that accounts for changes in the oxidation state (indicated by the O:C ratio) [*Donahue et al*., 2011, 2012]. The increases in the O:C ratio increase the likelihood that the SVOC will condense and increase the hygroscopicity of the OA formed [*Jimenez et al*., 2009]. These improvements include the VBS representation of biogenic SOA and anthropogenic SOA formation and the linking of the volatility of SOA to the hygroscopicity of the aerosol. Compared to the work of *He and Zhang* [2014], the version of CESM/CAM5.1-MAM7 used in this work includes the above updates and the aforementioned FN05 series parameterization for aerosol activation as implemented by *Gantt et al*. [2014].

3. Model Configurations and Evaluation Protocols

3.1. Model Setup and Inputs

The simulation is performed with fully coupled CESM1.0.5 with standard B_1850–2000_CAM5_CN configuration, which represents 1850–2000 transient conditions and includes all active component models in CESM with biogeochemistry in the land model. The simulation is conducted for 2001–2010 at a horizontal resolution of $0.9^\circ \times 1.25^\circ$ and a vertical resolution of 30 layers for CAM5.1.

The initial conditions for ice and ocean models are from CESM default settings. The initial conditions for the land model are based on the output from the NCAR CESM/CAM4 B_1850–2000_CN simulation. The initial

Table 2. Sources of Emission Inventories Used for 2001–2010 Simulation

Species[a]	Sources[b]	Spatial (Temporal) Resolution	Year	Available Domain
CO_2	*Zhang et al.* [2012]	1° × 1° (monthly)	2001	Global
	EDGAR v4.2	0.1° × 0.1° (annual)	2005/2008	Global
	MEIC	36 × 36 km (monthly)	2006/2010	China mainland
CO, NO_x, SO_2, NH_3, ALD2, ETH, ETHA, ETOH, FORM, IOLE, MEOH, OLE, PAR[d], TOL, XYL	*Zhang et al.* [2012][c]	1° × 1° (monthly)	2001	Global
	EDGAR v4.2	0.1° × 0.1° (annual)	2005/2008	Global
	MEIC	36 × 36 km (monthly)	2006/2010	China mainland
	AQMEII-CONUS	36 × 36 km (monthly)	2006/2010	CONUS
	AQMEII-EU	36 × 36 km (monthly)	2010	Europe
BC, OC	*Zhang et al.* [2012]	1° × 1° (monthly)	2001	Global
	EDGAR HTAPv1	0.1° × 0.1° (annual)	2005	Global
	EDGAR HTAPv2	0.1° × 0.1° (monthly)	2008	Global
	MEIC	36 × 36 km (monthly)	2006/2010	China mainland
	AQMEII-CONUS	36 × 36 km (monthly)	2006/2010	CONUS
	AQMEII-EU	36 × 36 km (monthly)	2010	Europe
CH_4, N_2O, AACD, CRES	*Zhang et al.* [2012]	1° × 1° (monthly)	2001	Global
	EDGAR v4.2	0.1° × 0.1° (annual)	2005/2008	Global
ALKH, PAH	RCP4.5	0.5° × 0.5° (monthly)	2000	Global
	EDGAR v4.2	0.1° × 0.1° (annual)	2005/2008	Global
CH_3Cl, $ClNO_2$, FMCL, CF_2ClBr, CF_3Br, CF_2Cl_2, $CFCl_3$, Hg(0), Hg(II)	*Zhang et al.* [2012]	1° × 1° (monthly)	2001	Global
DMS, H_2	*Zhang et al.* [2012]	1° × 1° (monthly)	2001	Global
	ACCMIP (biomass burning)	0.5° × 0.5° (monthly)	2005/2008	Global
HCl	*Zhang et al.* [2012]	1° × 1° (monthly)	2001	Global
	AQMEII-CONUS	36 × 36 km (monthly)	2006/2010	CONUS
Biogenic VOCs	*Guenther et al.* [2006]	Online	N/A	Global
Mineral dust	*Zender et al.* [2003]	Online	N/A	Global
Sea salt	*Martensson et al.* [2003]	Online	N/A	Global

[a] CO_2, carbon dioxide; CO, carbon monoxide; NO_x, nitrogen oxides (nitrogen dioxide (NO_2) + nitric oxide (NO)); SO_2, sulfur dioxide; NH_3, ammonia; ALD2, acetaldehyde; ETH, ethane; ETHA, ethane; ETOH, ethanol; FORM, formaldehyde; IOLE, internal olefinic carbon bond; MEOH, methanol; OLE, olefinic carbon bond; PAR, paraffin carbon bond; TOL, toluene; XYL, xylene; BC, black carbon; OC, organic carbon; CH_4, methane; N_2O, nitrous oxide; AACD, carboxylic acid; CRES, cresol and higher phenols; ALKH, long-chain alkanes; PAH, polycyclic aromatic hydrocarbons; CH_3Cl, methyl chloride; $ClNO_2$,chlorine nitrite; FMCL, formyl chloride; CF_2ClBr, chlorobromomethane; CF_3Br, trifluorobromomethane; CF_2Cl_2, dichlorodifluoromethane; $CFCl_3$, trichlorofluoromethane; Hg(0), mercury; Hg(II), mercury; DMS, dimethyl sulfide; H_2, hydrogen gas; HCl, hydrochloric acid; VOCs, volatile organic compounds.

[b] EDGAR, emission database for global atmospheric research; HTAP, hemispheric transport of air pollution; MEIC, multiresolution emission inventory for China; AQMEII, air quality modeling evaluation international initiative phase II; RCP, representative concentration pathway; ACCMIP, atmospheric chemistry and climate model intercomparison project; CONUS, continental U.S.

[c] Adjustment factors of 0.7, 0.5, and 1.2 for SO_2 emissions are applied over CONUS, Europe, and Asia, and 1.2 for emissions of NH_3, BC, and OC, and 1.3 for CO over all three regions.

[d] PAR = 0.955 × propane + 0.965 × butane + 0.972 × pentane + 0.117 × trimethylbenzene + 0.333 × propene.

conditions for CAM5.1 are derived from a 10 year (1990–2000) CAM5.1 standalone simulation with the MOZART chemistry provided by NCAR. A 1 year (1 January to 31 December 2000) CESM/CAM5.1 simulation using the NCAR CESM B_1850–2000_CAM5_CN component set is performed as a spin-up to provide the initial conditions for the meteorological variables and chemical species that are treated in both MOZART and CB05_GE. An additional 3 month (1 October to 31 December 2000) CESM/CAM5.1 simulation based on a 10 month (January–October 2000) CESM/CAM5.1 output using initial conditions from NCAR's CESM B_1850–2000_CAM5_CN is performed as a spin-up to provide initial conditions for chemical species that are treated in CB05_GE but not in MOZART.

Table 2 shows the emission inventories that are used for the 2001–2010 simulations. The emissions representative of three time periods are used for the CESM simulations of 2001–2003, 2004–2006, and 2007–2010, respectively. Emissions for the first period are based on *Zhang et al.* [2012] with adjustment factors of 0.7, 0.5, and 1.2 for sulfur dioxide (SO_2) over the continental U.S. (CONUS), Europe, and East Asia, respectively, and 1.2 for ammonia (NH_3), black carbon (BC), and organic carbon (OC), and 1.3 for carbon monoxide (CO) over all three regions. Those emissions are adjusted based on the comparison with several global emission inventories and preliminary evaluation of the NCSU CESM/CAM5.1 against available observations. Emissions for the second period are based on the 2005 Emission Database for Global Atmospheric Research (EDGAR), with regional updates based on the 2006 emissions from Air Quality Modeling Evaluation International Initiative Phase II (AQMEII) over North America and the 2006 emissions from the Multiresolution Emission Inventory for China (MEIC) over China. Emissions for the third period are based on the 2008 EDGAR

emissions, with regional updates from the 2010 AQMEII emissions over North America and Europe, and from the 2010 MEIC emissions over China. The emissions for missing species in EDGAR (e.g., dimethyl sulfide (DMS) and hydrogen gas (H_2)) are based on *Zhang et al*. [2012] with inclusion of DMS and H_2 emissions from biomass burning, which are from the Atmospheric Chemistry and Climate Model Intercomparison Project (ACCMIP). The online emissions include those of biogenic VOCs simulated with the Model of Emissions of Gases and Aerosols from Nature version 2 (MEGAN 2) [*Guenther et al*., 2006], mineral dust [*Zender et al*., 2003], and sea salt [*Martensson et al*., 2003].

The simulation includes a total of 139 prognostic species in tracer advection. The simulation calculates photolysis rates based on *Lamarque et al*. [2012] and uses the aqueous-phase chemistry described by *He and Zhang* [2014]. Major physical options include the cloud microphysics parameterization of *Morrison and Gettelman* [2008], the moisture PBL scheme of *Bretherton and Park* [2009], the shallow and deep convection schemes of *Park and Bretherton* [2009] and *Zhang and McFarlane* [1995], respectively, and the Rapid Radiative Transfer Model for GCMs (RRTMG) of *Mlawer et al*. [1997] and *Iacono et al*. [2003, 2008] for long and shortwave radiation. The land surface processes are simulated by the Community Land Model (CLM) of *Lawrence et al*. [2011] in CESM that is coupled with CAM5.1. A sensitivity simulation of 2001–2010 using CESM-CAM5 with the same configurations as baseline but with 80% reductions in the anthropogenic emissions is also conducted. The results from this sensitivity simulation are compared with the baseline simulation to quantify the impacts of chemical species including both gases and aerosol species on climate through various feedbacks mechanisms.

3.2. Available Measurements

A number of observational data sets from surface networks and satellites are used for model evaluation. They are summarized along with the variables to be evaluated in Table 3. Global surface networks include the National Climatic Data Center (NCDC), the Global Precipitation Climatology Project (GPCP), and the National Oceanic and Atmospheric Administration Climate Diagnostics Center (NOAA/CDC). The National Centers for Environmental Prediction (NCEP) reanalysis data are from a joint project between the NCEP and NCAR. The satellite data sets include the Moderate Resolution Imaging Spectroradiometer (MODIS), the Clouds and Earth's Radiant Energy System (CERES), the Total Ozone Mapping Spectrometer/the Solar Backscatter UltraViolet (TOMS/SBUV), the Aura Ozone Monitoring Instrument in combination with Aura Microwave Limb Sounder (OMI/MLS), the Measurements Of Pollution In The Troposphere (MOPITT), the Global Ozone Monitoring Experiment (GOME), and the SCanning Imaging Absorption spectroMeter for Atmospheric CHartographY (SCIAMACHY). Other satellite-based data include the MODIS-derived cloud droplet number concentration (CDNC) and cloud liquid water path (LWP) from the University of Wisconsin-Madison (UW-M), which are derived based on *Bennartz* [2007].

Regional observational networks include the Clean Air Status and Trends Network (CASTNET), the Interagency Monitoring of Protected Visual Environments (IMPROVE), and the Speciation Trends Network (STN) over CONUS; the European Monitoring and Evaluation Program (EMEP), the Base de Données sur la Qualité de l'Air (BDQA), and the European air quality database (AirBase) over Europe; the Ministry of Environmental Protection of China (MEPC), the National Institute for Environmental Studies of Japan (NIESJ), Taiwan Air Quality Monitoring Network (TAQMN), and the Korean Ministry Of Environment (KMOE) over East Asia. Traffic and industrial sites from AirBase and BDQA are excluded for the chemical evaluation because the horizontal grid resolution used in this work is too coarse to reproduce observations at those sites.

3.3. Evaluation Protocols

The protocols for performance evaluation include spatial distributions and statistics, following the approach of *Zhang et al*. [2012]. The analysis of the performance statistics focuses on mean bias (MB), normalized mean bias (NMB), normalized mean error (NME), root mean square error (RMSE), and correlation coefficient (Corr.). The meteorological and radiative variables are evaluated annually or seasonally, including temperature at 2 m (T2), specific humidity at 2 m (Q2), and wind speed at 10 m (WS10) from NCDC; vertical temperature profile, vertical relative humidity (RH) profile, and vertical specific humidity (Q) profile from NCEP/NCAR reanalysis data; total daily precipitation rate (Precip) from GPCP; outgoing longwave radiation (OLR) from NOAA/CDC; downwelling shortwave radiation (FSDS), downwelling longwave radiation (FLDS), surface net shortwave flux (FSNS), surface net longwave flux (FLNS), shortwave cloud forcing (SWCF), and longwave cloud forcing (LWCF) from CERES; cloud fraction (CF), aerosol optical depth (AOD), cloud optical thickness

Table 3. Data Sets for Model Evaluation[a]

Species/Variables	Data Set
Temperature at 2 m (T2), specific humidity at 2 m (Q2), wind speed at 10 m (WS10)	NCDC
Vertical temperature profile (T), vertical relative humidity profile (RH), vertical specific humidity profile (Q)	NCEP/NCAR
Precipitation (Precip)	GPCP
Outgoing longwave radiation (OLR)	NOAA/CDC
Cloud fraction (CF), cloud optical thickness (COT), precipitating water vapor (PWV), aerosol optical depth (AOD), column cloud condensation nuclei (ocean) at S = 0.5% (CCN5)	MODIS
Cloud droplet number concentration (CDNC), cloud liquid water path (LWP)	UW-M
Downwelling longwave radiation (FLDS), downwelling shortwave radiation (FSDS), surface net longwave flux (FLNS), surface net shortwave flux (FSNS), shortwave cloud radiative forcing (SWCF), longwave cloud radiative forcing (LWCF)	CERES
Carbon monoxide (CO)	East Asia: NIESJ, TAQMN, KMOE
Ozone (O_3)	CONUS: CASTNET Europe: Airbase, BDQA, EMEP East Asia: TAQMN, KMOE
Sulfur dioxide (SO_2)	CONUS: CASTNET Europe: Airbase, BDQA, EMEP East Asia: NIESJ, TAQMN, KMOE
Nitric acid (HNO_3)	CONUS: CASTNET Europe: EMEP
Ammonia (NH_3)	Europe: EMEP
Nitrogen dioxide (NO_2)	Europe: Airbase, BDQA, EMEP East Asia: NIESJ, TAQMN, KMOE
Sulfate (SO_4^{2-}), ammonium (NH_4^+), nitrate (NO_3^-), chloride (Cl^-)	CONUS: CASTNET, IMPROVE, STN Europe: EMEP
Organic carbon (OC)	CONUS: IMPROVE
Black carbon (BC), total carbon (TC)	CONUS: IMPROVE, STN
Particulate matter with diameter less than 2.5 μm ($PM_{2.5}$)	CONUS: IMPROVE, STN Europe: Airbase, BDQA, EMEP
Particulate matter with diameter less than 10 μm (PM_{10})	Europe: Airbase, BDQA, EMEP East Asia: MEPC, NIESJ, TAQMN, KMOE
Tropospheric CO	Globe: MOPITT
Tropospheric SO_2, HCHO	Globe: SCIAMCHY
Tropospheric NO_2	Globe: GOME, SCIAMCHY
Tropospheric ozone residual (TOR)	Globe: TOMS/SBUV, OMI/MLS

[a]NCDC: National Climatic Data Center; NCEP/NCAR: National Centers for Environmental Prediction and National Center for Atmospheric Research; GPCP: Global Precipitation Climatology Project; NOAA/CDC: National Oceanic and Atmospheric Administration Climate Diagnostics Center; MODIS: Moderate Resolution Imaging Spectroradiometer; UW-M: University of Wisconsin-Madison; CERES: Clouds and Earth's Radiant Energy System; TOMS/SBUV: the Total Ozone Mapping Spectrometer/the Solar Backscatter UltraViolet; OMI/MLS: the Aura Ozone Monitoring Instrument in combination with Aura Microwave Limb Sounder; MOPITT: the Measurements Of Pollution In The Troposphere; the Global Ozone Monitoring Experiment; SCIAMCHY: the SCanning Imaging Absorption spectroMeter for Atmospheric CHartographY; GOME: the Global Ozone Monitoring Experiment; CASTNET: Clean Air Status and Trends Network; IMPROVE: Interagency Monitoring of Protected Visual Environments; STN: Speciation Trends Network; EMEP: European Monitoring and Evaluation Program; BDQA: Base de Données sur la Qualité de l'Air; AirBase: European air quality database; MEPC: Ministry of Environmental Protection of China; TAQMN: Taiwan Air Quality Monitoring Network; NIESJ: National Institute for Environmental Studies of Japan; KMOE: Korean Ministry of Environment.

(COT), precipitating water vapor (PWV), and CCN from MODIS; and CDNC and LWP from UW-M. CDNC is calculated as an average value of layers between 850 and 960 mb for comparison with the satellite-derived values of UW-M. Surface chemical predictions are evaluated against various observational sites from each network (see Table 3). Chemical concentrations evaluated include seasonal and annual averaged concentrations of CO, ozone (O_3), SO_2, NH_3, nitrogen dioxide (NO_2), HNO_3, particulate matter (PM) with aerodynamic diameter less than 10 μm (PM_{10}) and 2.5 μm ($PM_{2.5}$), and its major components (i.e., SO_4^{2-}, NO_3^-, NH_4^+, BC, OC, and total carbon (TC) for CONUS and Europe). The chemical observations over East Asia are very limited and only include surface concentrations of CO, SO_2, NO_2, O_3, and PM_{10}. Column concentrations of tropospheric CO, NO_2, SO_2, and formaldehyde (HCHO), and tropospheric O_3 residual (TOR) are evaluated for the globe. Following the regions suggested by *Rausch et al*. [2010], interannual variations of PM, column CCN at supersaturation of 5% (CCN5), AOD, and SWCF are analyzed over the marine stratocumulus regions of near Australia (AUS, 30°S–40°S, 88°E–103°E), North America (NAM, 15°N–35°N, 115°W–140°W), South East Asia (SEA, 0°N–40°N, 105°W–150°W), Southern Africa (SAF, 5°S–25°S, 10°W–15°E), and South America (SAM, 8°S–28°S, 70°W–90°W).

Model performance is also compared with CESM1-CAM5 ensemble simulations under historical and Representative Concentration Pathway (RCP) 4.5 scenarios from CMIP5. All observational data used for evaluating 2001–2010 simulations were based on 2001–2010 except for several variables with data during a limited time period including LWP from UW-M (2001–2008), chemical observations from KMOE (2006–2010), tropospheric SO_2 from SCIAMACHY (2005–2010), tropospheric HCHO from GOME (2001–2002) and SCIAMACHY (2003–2010), TOR from TOMS/SBUV (2001–2004) and OMI/MLS (2005–2010), and tropospheric NO_2 from GOME (2001–2002) and SCIAMACHY (2003–2010).

4. Model Evaluation and Intercomparison

4.1. Evaluation of Improved CESM/CAM5.1

4.1.1. Meteorology and Radiation Evaluation

Table 4 shows the statistical performance for major meteorological and radiative variables, and Figure 1 shows the absolute differences between model simulation and observations/reanalysis data averaged for 2001–2010. Compared with NCDC observations, meteorological variables such as T2, Q2, and WS10 are underpredicted by 2.9°C ($\sim -22.1\%$), 1.0 g kg^{-1} ($\sim -11.4\%$), and 0.4 m s^{-1} ($\sim -9.7\%$), respectively, whereas Precip is overpredicted by 0.1 mm d^{-1} ($\sim$6.6%), with a correlation coefficient of 0.5–0.9. Compared with NCEP data, meteorological variables such as T2 and Q2 are underpredicted by 2.6°C ($\sim -45.1\%$) and 1.3 g kg^{-1} ($\sim -15.8\%$), respectively, whereas WS10 is overpredicted by 2.5 m s^{-1} ($\sim$58.4%). The underprediction of T2 is mainly due to the underprediction of the heat flux at the surface. As shown in Figure 1, there are large discrepancies for T2 between model simulation and the NCEP/NCAR reanalysis data, especially over higher latitudes. There is a large cold bias (>5°C) between 60°N and 90°N, whereas there is a warm bias between 50°S and 70°S. The T2 biases are less than 2°C over most continental areas and oceanic areas in the low and middle latitudes. The large underprediction of T2 over higher latitudes is due to the inaccurate predictions of the net flux (FSNS + FLNS) at the surface. Since FSNS represents the heating effect and FLNS represents the cooling effect, the combination of underpredicted FSNS (by 4.8%) and overpredicted FLNS (by 5.7%) contributes to the further underprediction of T2. Compared with NCEP/NCAR reanalysis data, Q2 is underpredicted by 0.5–4.9 g kg^{-1} (1–15%) over most regions except for the Sahara desert, western Asia, Australia, and the western U.S., whereas WS10 is overpredicted by 0.5–7.3 m s^{-1} (20–200%) over most regions especially over oceanic areas in the middle and higher latitudes. Figures 2a and 2b compare meteorological variables with NCEP over North America, South America, Africa, Asia, Europe, and Australia for December-January-February (DJF) and June-July-August (JJA), respectively. Temperature profiles from CESM agree reasonably well with NCEP for both JJA and DJF, despite some discrepancies near the surface for some regions. For example, the temperature near the surface (925 mb) from CESM is about 4°C lower than NCEP over Asia (JJA and DJF), Africa (DJF), and North America (DJF). For other regions, the temperature differences are less than 4°C. Specific humidity profiles from CESM agree very well with NCEP for both JJA and DJF over six regions although there are discrepancies (<1.2 g kg^{-1}) near the surface over Asia, Europe, and North America in JJA. The underprediction of Q2 is likely due to the overprediction of Precip. There are large discrepancies for relative humidity (RH) profiles between CESM and NCEP although their distribution patterns are similar. RH from CESM is overall higher than that from NCEP. The overprediction of RH is likely due to the underprediction of temperature and overprediction of moisture fluxes from overprediction of Precip. The different performance of WS10 against NCDC and NCEP is mainly due to different data pairs used in the model evaluation as well as the different degrees of uncertainties in the observations and reanalysis data. Due to the limited observations, observational sites in NCDC do not cover the entire global domain whereas NCEP data cover each grid cell. It is possible that some grid cells with large biases in NCEP are not taken into account in NCDC due to the unavailability of observations. On the other hand, reanalysis data are processed in global forecast models based on multiple sources of observations. Uncertainties in observations and model treatments can propagate to the reanalysis data. *Smith et al.* [2001] showed that there was a significant underestimation in near-surface wind speed by NCEP reanalysis data, which can partly explain the overpredictions of WS10.

Radiative variables such as OLR, FSDS, FLNS, FLDS, and FSNS show excellent agreement with observations, with NMBs within $\pm$6%; and SWCF and LWCF show reasonably good agreement, with NMBs of 10.6 and $-$19%, respectively. All predicted radiation variables show high correlation with observations, with Corr. values of 0.9–0.99. While CF is well predicted, moderate overpredictions or underpredictions occur for CDNC,

Table 4. Statistical Performance of Meteorological/Radiative Variables and Chemical Species

		Obs	Sim	MB[a]	NMB (%)[a]	NME (%)[a]	RMSE[a]	Corr[a]
Meteorological/Radiative Variables								
T2 (°C)	NCDC[b]	13.1	10.2	−2.9	−22.2	28.0	4.8	0.9
	NCEP/NCAR[c]	5.7	3.2	−2.6	−45.1	51.1	4.1	0.99
Q2 (g kg^{-1})	NCDC	8.3	7.3	−1.0	−11.4	17.4	1.9	0.9
	NCEP/NCAR	8.3	7.0	−1.3	−15.8	17.2	1.6	0.99
WS10 (m s^{-1})	NCDC	3.7	3.3	−0.4	−9.7	32.8	1.8	0.5
	NCEP/NCAR	4.3	6.8	2.5	58.4	64.3	3.3	0.6
Precip (mm d^{-1})	GPCP	2.3	2.4	0.1	6.6	26.0	1.0	0.9
OLR (W m^{-2})	NOAA/CDC	216.4	217.9	1.4	0.7	2.9	7.8	0.98
FLDS (W m^{-2})	CERES	306.3	292.6	−13.8	−4.5	4.8	18.4	0.99
FSDS (W m^{-2})	CERES	163.5	161.8	−1.7	−1.0	6.6	14.0	0.97
FLNS (W m^{-2})	CERES	−47.6	−50.3	2.7	5.7	14.2	9.0	0.9
FSNS (W m^{-2})	CERES	128.5	122.4	−6.2	−4.8	7.9	13.4	0.99
SWCF (W m^{-2})	CERES	−40.7	−45.1	4.3	10.6	26.3	14.5	0.9
LWCF (W m^{-2})	CERES	22.7	18.3	−4.4	−19.4	24.0	6.5	0.9
CCN5[d] (# cm^{-2})	MODIS	2.4×10^{8}	4.3×10^{7}	-2.0×10^{8}	−82.2	82.2	4.8×10^{8}	0.1
CF (%)	MODIS	67.2	67.5	0.3	0.4	15.3	13.6	0.7
COT	MODIS	17.0	9.9	−7.1	−41.7	57.8	13.6	−0.2
AOD	MODIS	1.6×10^{-1}	1.0×10^{-1}	-5.5×10^{-2}	−35.4	49.2	0.1	0.6
PWV (cm)	MODIS	1.9	1.7	−0.2	−10.5	17.2	0.5	0.98
CDNC (# cm^{-3})	UW-M	108.5	140.5	29.0	26.7	52.2	74.1	0.4
LWP (g m^{-2})	UW-M	85.7	59.0	−26.7	−31.2	34.2	38.3	0.5
		Obs	Sim	MB	NMB (%)	NME (%)	RMSE	Corr
Chemical Species								
CO (ppm)	East Asia	503.9	221.2	−282.7	−56.1	56.4	315.9	0.4
SO_2[e]	CONUS	2.7	8.7	6.0	219.1	219.6	9.5	0.8
	Europe	5.5	5.2	−0.3	−5.2	65.9	6.5	0.4
	East Asia	3.2	2.6	−0.6	−18.2	65.9	3.6	0.3
NH_3 (μg m^{-3})	Europe	1.0	1.3	0.3	31.9	75.2	1.0	0.5
NO_2[f]	Europe	18.6	4.1	−14.4	−77.7	78.6	17.4	0.2
	East Asia	12.8	2.2	−10.6	−82.7	83.0	11.7	0.5
O_3[g]	CONUS	35.1	40.8	5.7	16.2	20.6	9.0	0.5
	Europe	54.9	81.2	26.2	47.8	48.7	29.0	0.3
	East Asia	28.7	42.6	13.9	48.5	49.1	15.7	0.2
HNO_3 (μg m^{-3})	CONUS	1.2	1.8	0.6	48.5	60.1	0.9	0.6
	Europe	0.8	1.1	0.3	41.8	84.0	0.9	0.2
Col. CO (molecules cm^{-2})	Globe	1.4×10^{18}	2.6×10^{18}	1.2×10^{18}	84.3	84.3	1.3×10^{18}	0.8
Col. NO_2 (molecules cm^{-2})	Globe	5.0×10^{14}	7.2×10^{14}	1.9×10^{14}	35.5	52.2	4.5×10^{14}	0.9
Col. HCHO (molecules cm^{-2})	Globe	4.2×10^{15}	2.3×10^{15}	-1.9×10^{15}	−44.6	48.0	2.7×10^{15}	0.6
Col. SO_2 (DU)	Globe	0.2	0.1	−0.1	−28.4	113.3	0.4	−0.1
TOR (DU)	Globe	29.1	28.1	−1.0	−3.5	16.8	5.7	0.8
SO_4^{2-} (μg m^{-3})	CONUS	2.3	2.0	−0.3	−12.8	24.3	0.8	0.9
	Europe	2.0	1.6	−0.4	−20.8	36.7	1.0	0.6
NH_4^+ (μg m^{-3})	CONUS	1.1	1.5	0.4	37.4	53.2	0.9	0.7
	Europe	0.9	1.5	0.5	59.8	68.0	0.8	0.8
NO_3^- (μg m^{-3})	CONUS	1.0	2.0	1.0	93.2	118.3	1.9	0.5
	Europe	1.8	2.7	0.8	44.8	72.3	1.9	0.6
Cl^- (μg m^{-3})	CONUS	0.1	0.1	-3.2×10^{-3}	−3.0	100.3	0.4	0.2
	Europe	0.9	4.4	3.5	376.0	376.0	4.6	0.7
BC (μg m^{-3})	CONUS	0.4	0.3	-5.7×10^{-2}	−15.6	44.3	0.3	0.5
OC (μg m^{-3})	CONUS	1.1	1.1	-2.2×10^{-2}	−2.0	46.7	0.8	0.4
TC (μg m^{-3})	CONUS	2.6	1.6	−1.0	−37.9	49.9	2.1	0.5
$PM_{2.5}$ (μg m^{-3})	CONUS	8.4	8.3	−0.1	−1.1	31.3	3.6	0.7
	Europe	13.6	9.8	−3.9	−28.2	36.4	7.7	0.3
PM_{10} (μg m^{-3})	Europe	23.1	21.7	−1.5	−6.3	38.5	13.6	0.2
	East Asia	97.1	60.9	−36.1	−37.2	43.0	49.2	0.6

[a]MB: mean bias; NMB: normalized mean bias (%); NME: normalized mean error (%); RMSE: root mean squared error; Corr.: correlation coefficient.
[b]Results are based on NCDC sites mean.
[c]Results are based on global mean.
[d]Column CCN (ocean) at supersaturation of 0.5%.
[e]The unit is μg m^{-3} for CONUS and Europe, and ppb for East Asia.
[f]The unit is μg m^{-3} for Europe and ppb for East Asia.
[g]The unit is ppb for CONUS and East Asia, and μg m^{-3} for Europe.

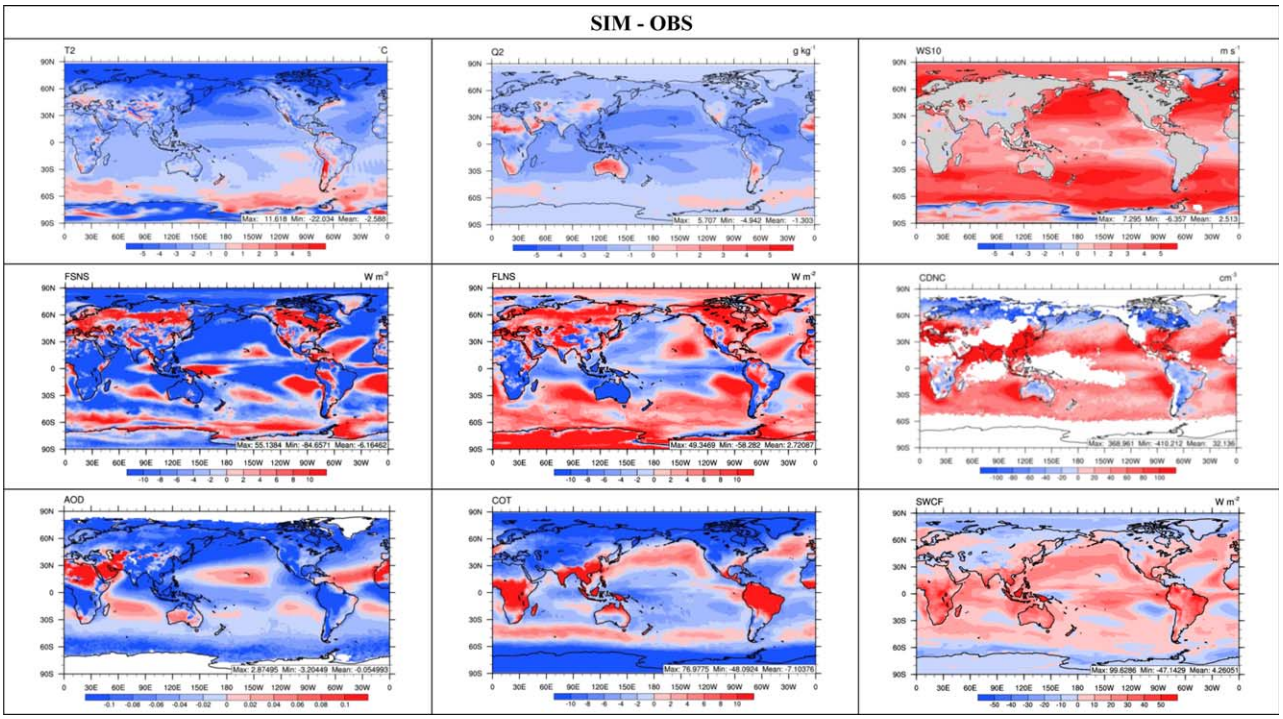

Figure 1. Absolute differences between simulation results from CESM_NCSU and observations/reanalysis for 2001–2010. NCEP reanalysis data are used for comparison of T2, Q2, and WS10. CERES data are used for comparison of FSNS, FLNS, and SWCF. UW-M data are used for comparison of CDNC. MODIS data are used for comparison of AOD and COT.

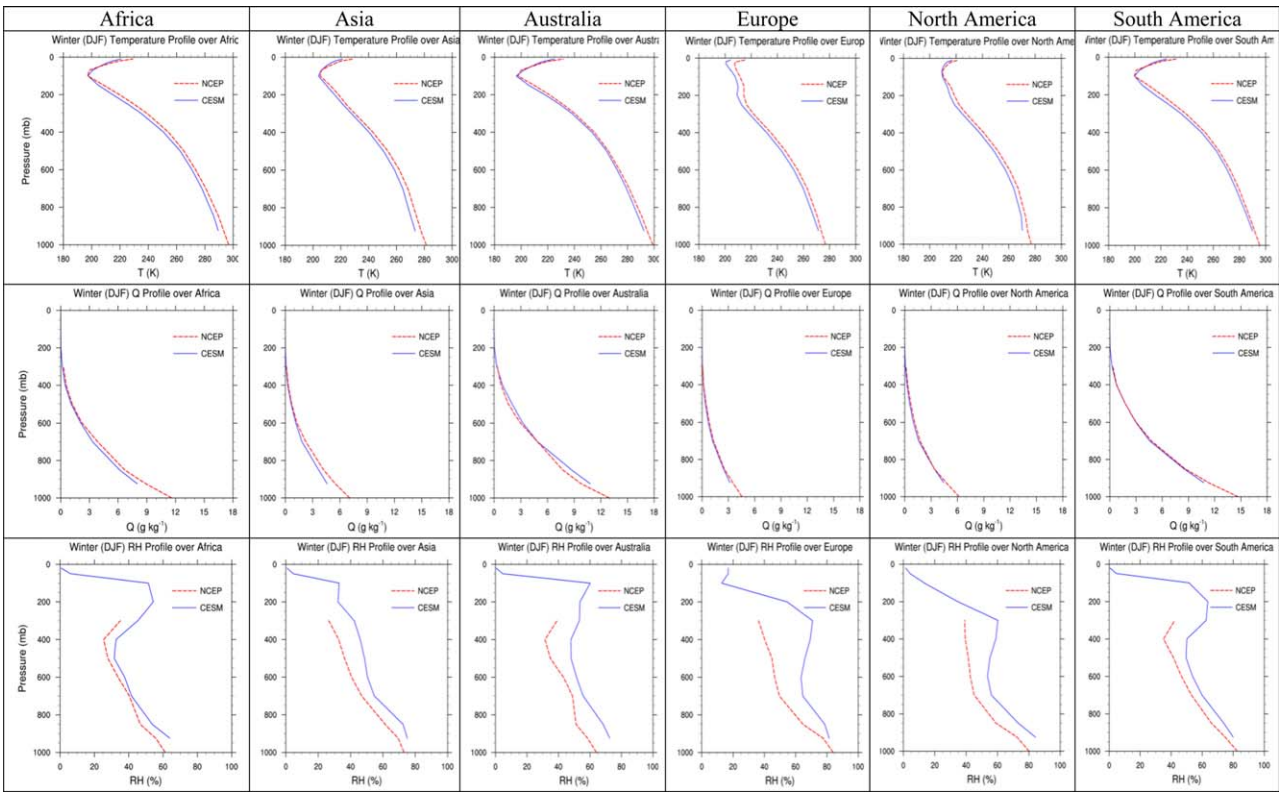

Figure 2. (a) Comparison of meteorological profiles of CESM-NCSU with NCEP over Africa, Asia, Australia, Europe, North America, and South America for December, January, and February (DJF). (b) Comparison of meteorological profiles of CESM-NCSU with NCEP over Africa, Asia, Australia, Europe, North America, and South America for June, July, and August (JJA).

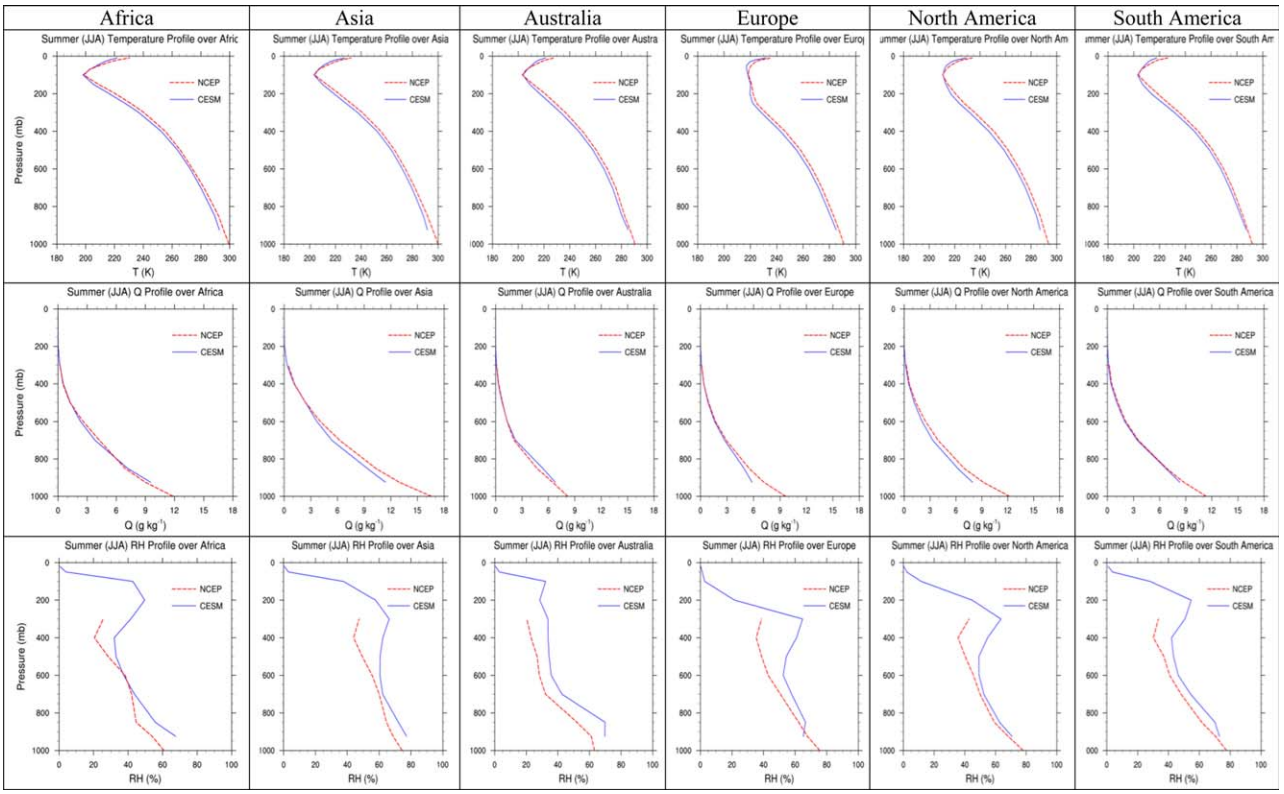

Figure 2. (continued)

AOD, COT, and LWP, with NMBs of 26.7, −35.4, −41.7, and −31.2%, respectively, and large underpredictions occur for column CCN5 over oceanic areas with an NMB of −82.2%. Due to the underpredictions of cloud variables (e.g., COT, LWP, and CCN5), OLR is slightly overpredicted by 1.4 W m^{-2} (or by 0.7%) and LWCF is underpredicted by 4.4 W m^{-2} (or by 19.4%). As shown in Figure 1, CDNC is largely overpredicted by 40–369 cm^{-3} (or by 40–752%) over most oceanic areas, East Asia, Europe, and eastern U.S. Cloud droplet formation is sensitive to both particle number concentration and updraft velocity [*Reutter et al*., 2009]. The overprediction of CDNC is due partly to high activation fractions (e.g., inclusion of adsorption activation from insoluble CCN and effective uptake coefficient of 0.06 used in this work) [*Gantt et al*., 2014] as well as the uncertainties in the model treatments for cloud microphysics (e.g., resolved clouds and subgrid-scale cumulus clouds) and satellite retrievals (e.g., error propagation of the input variables to derive CDNC) [*Bennartz*, 2007]. For example, a constant condensation coefficient of water vapor with a value of 0.06 is used to determine size-dependent water vapor diffusivity in FN05. However, this value is uncertain and may vary by a factor of five for pure water (i.e., 0.1–0.3) [*Ghan et al*., 2011; FN05]. It varies from 0.04 to 0.06 for aged atmospheric droplet and can be further reduced by the presence of organic films [*Chuang*, 2003; *Ghan et al*., 2011; FN05]. In K09, empirical constants of A_{FHH} (e.g., 2.25 used in this work) and B_{FHH} (e.g., 1.20 used in this work) are used to determine the water vapor saturation ratio of an insoluble particle in equilibrium with surrounding water vapor. However, A_{FHH} and B_{FHH} have been found to vary from 0.1 to 3.0 and from 0.5 to 3.0, respectively, from experimental studies [*Sorjamaa and Laaksonen*, 2007; K09]. Therefore, these constant parameters used in this work may contribute to the uncertainties in predicting CDNC. On the other hand, MODIS is known to provide very high values for the retrieved effective radius, especially over those remote oceanic areas that are dominated by broken cumulus clouds. This possibly is a retrieval artifact caused by cloud inhomogeneites [*Zhang and Platnick*, 2011] or drizzle/rain contamination [*Nakajima et al*., 2010]. Such a high bias in effective radius would result in an underestimation of MODIS-derived CDNC, which is based on the retrieved MODIS effective radii [*Bennartz*, 2007]. The statistical evaluation of CDNC over land and oceanic areas indicates that most overpredictions occur over ocean, due mainly to the underestimated MODIS-CDNC. The underpredictions of AOD over oceanic areas can be attributed to the

uncertainties in the sea-salt emissions as well as inaccurate predictions of other PM components (e.g., marine organic aerosols) over the ocean and overestimation of oceanic AOD in the MODIS collection 5.1 [*Levy et al*., 2013]. COT is largely overpredicted by 5–77 (or by 20–529%) over Southeast Asia, South Africa, South America, and northern Australia, and slightly overpredicted over western Europe and eastern U.S., whereas it is largely underpredicted by 10–48 (or by 50–100%) over continents of 50°N–90°N and regions within 60°S–90°S. Overpredictions in CDNC and COT can increase cloud albedo and, therefore, increase SWCF, leading to its overpredictions by 10–99.6 W m^{-2} (or by 20–250%) mainly over the low and middle latitudes. The underpredictions in COT and LWP may be caused by limitations and uncertainties associated with the microphysics treatments for resolved and cumulus clouds. The large underpredictions of LWP and COT over polar regions can be also attributed to the uncertainties in plane-parallel visible-near-infrared retrievals with low solar zenith angle [*Seethala and Horváth*, 2010] as well as the influence of radiatively active snow on overlying cloud fraction [*Kay et al*., 2012]. Underpredictions in COT can decrease SWCF as well, leading to underpredictions of SWCF over higher latitudes. The opposite performance of CDNC (overprediction) and COT (underprediction) is likely due to the fact that COT (i.e., mixed-phase clouds) is affected by both aerosol activation and ice nucleation [*Lance et al*., 2011; *Xie et al*., 2013]. CDNC is evaluated between 850 and 950 mb, whereas COT is evaluated over entire model layers. Uncertainties in ice clouds predictions can result in uncertainties in COT predictions. The moderate and poor correlation coefficients of cloud variables (e.g., CCN5, COT, CDNC, and LWP) suggest the uncertainties both in the model treatments for microphysics and in the satellite retrievals.

Figures 3–5 compare AOD, CDNC, and SWCF with observations for the 10 year average of 2001–2010 (ANU), December-January-February (DJF), March-April-May (MAM), June-July-August (JJA), and September-October-November (SON). AOD is underpredicted over most regions except North Africa, the tropical Atlantic Ocean, and West Asia for MAM, JJA, and SON. The model captures the hot spots for observed AOD over East Asia, North Africa, the tropical Atlantic Ocean, and West Asia (e.g., in MAM and JJA), whereas it fails to predict the hot spot for South Africa in SON. The hot spots for AOD are mainly due to the high concentration of dust, indicating the uncertainties in the dust emissions. The underprediction of AOD over 40°S–70°S is mainly due to a bias in satellite products (i.e., MODIS Collection 5.1), which does not account for the wind speed-dependent whitecap and foam fraction on the ocean surface [*Levy et al.* 2013]. Unlike AOD, CDNC is overpredicted over most regions. The model can also capture the hot spots for observed CDNC over Europe, East Asia, and East U.S. (e.g., in DJF, MAM, and SON). The hot spots for CDNC are mainly due to the high PM concentrations over those regions. The overpredictions of CDNC are likely due to uncertainties in the treatment of insoluble CCN activations (e.g., BC and dust) and effective uptake coefficient used for aerosol activation as well as the uncertainties in the model treatments for cloud microphysics (e.g., resolved clouds and subgrid-scale cumulus clouds) and satellite retrievals as discussed previously. Similar to CDNC, SWCF is also overpredicted in all seasons especially over oceanic areas in low and middle latitudes as well as land areas such as East Asia, eastern U.S., Europe, South America, South Africa, and Australia. Due to the overpredictions of CDNC over these regions, cloud albedo increases and more solar radiation is reflected, resulting in overpredictions of SWCF. However, SWCF over polar regions is underpredicted, especially in JJA. The underpredictions of SWCF over the polar regions are likely due to the underpredictions of COT over those regions (see Figure 1).

4.1.2. Chemical Species Evaluation

Table 4 shows the statistical performance for major chemical species, and Figure 6 compares simulated and observed surface concentrations of chemical species over various sites from different surface networks including CASTNET, IMPROVE, EMEP, MEPC, TAQMN, and NIESJ. CO mixing ratios and NO_2 concentrations over East Asia are largely underpredicted with NMBs of −56.1 and −82.7%, respectively; these results are likely due to uncertainties in the CO and NO_x emissions over this region. SO_2 concentrations are moderately underpredicted with absolute NMBs less than 20% over Europe (but the NMBs can be as high as 244.7% over the EMEP sites as shown in Figure 6) and East Asia (with an NMB of 18% over the NIESJ sites), but largely overpredicted with an NMB of 219.1% over CONUS (with an NMB of 244.7% over the CASTNET sites), which is likely due to uncertainties in the SO_2 emissions and wet deposition, and measurements. *He and Zhang* [2014] investigated the sensitivity of the chemical predictions to emissions; the results showed that with a 30% reduction in SO_2 emissions, the NMB of SO_2 predictions is reduced by about half, from 291.8 to 152.2%. Precip is also underpredicted over the middle/eastern U.S., resulting in less SO_2 wet deposition.

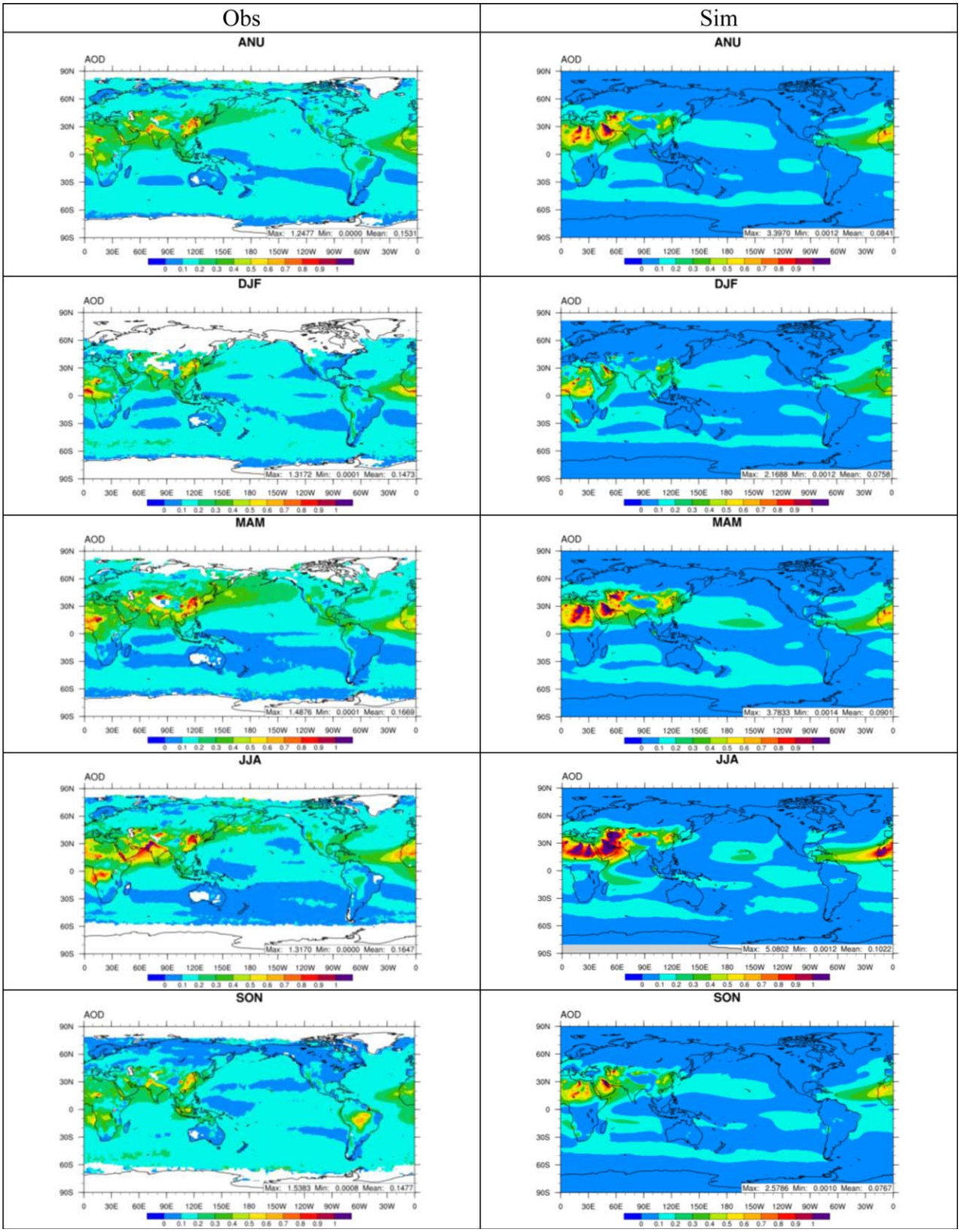

Figure 3. Seasonal and annual comparison of simulated AOD (Sim.) against MODIS observations (Obs.). From top to bottom: annual (ANU), December-January-February (DJF), March-April-May (MAM), June-July-August (JJA), and September-October-November (SON). The results are based on 10 year average of 2001–2010.

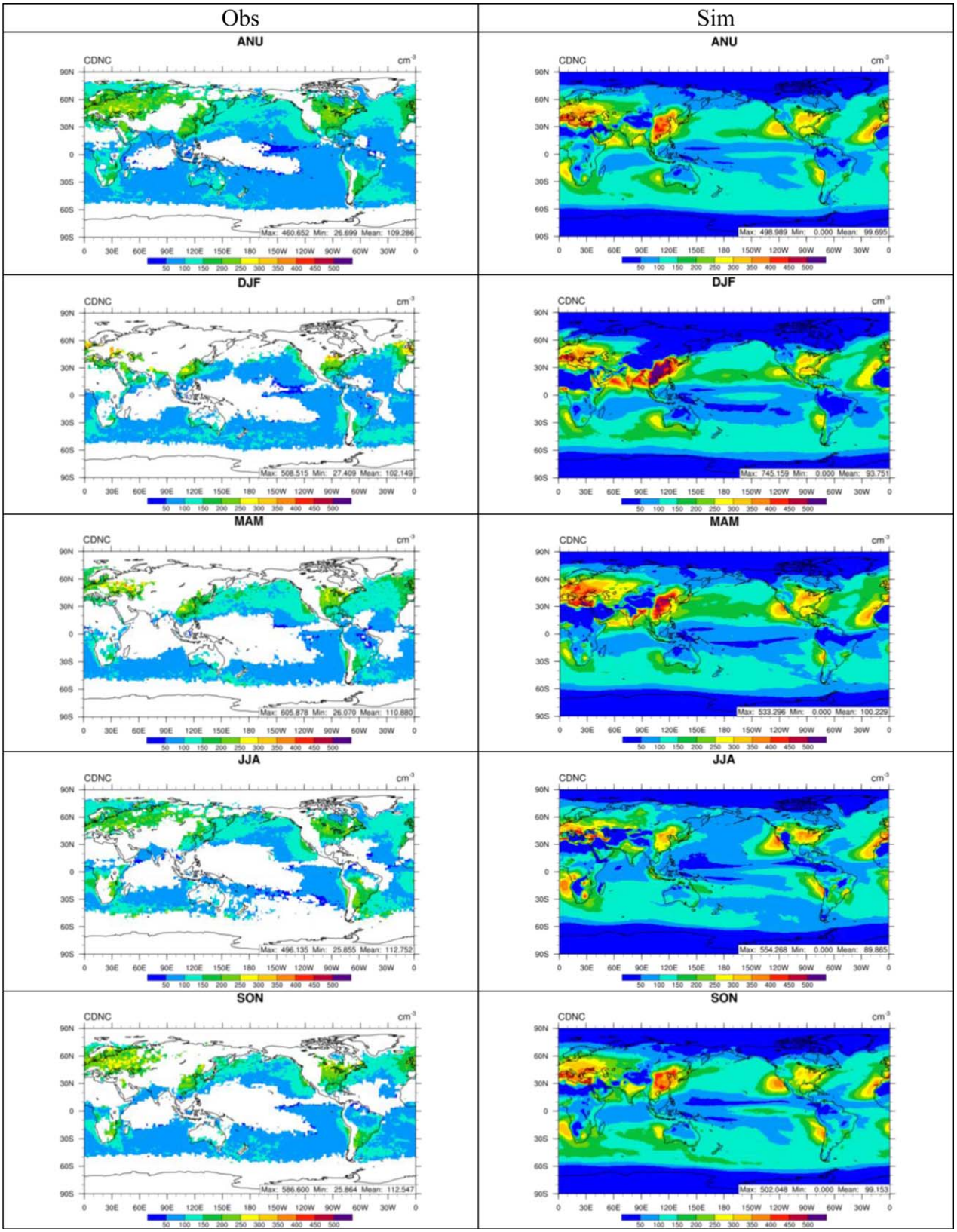

Figure 4. Seasonal and annual comparison of simulated CDNC (Sim.) against UW-M observations (Obs.). From top to bottom: annual (ANU), December-January-February (DJF), March-April-May (MAM), June-July-August (JJA), and September-October-November (SON). The results are based on 10 year average of 2001–2010.

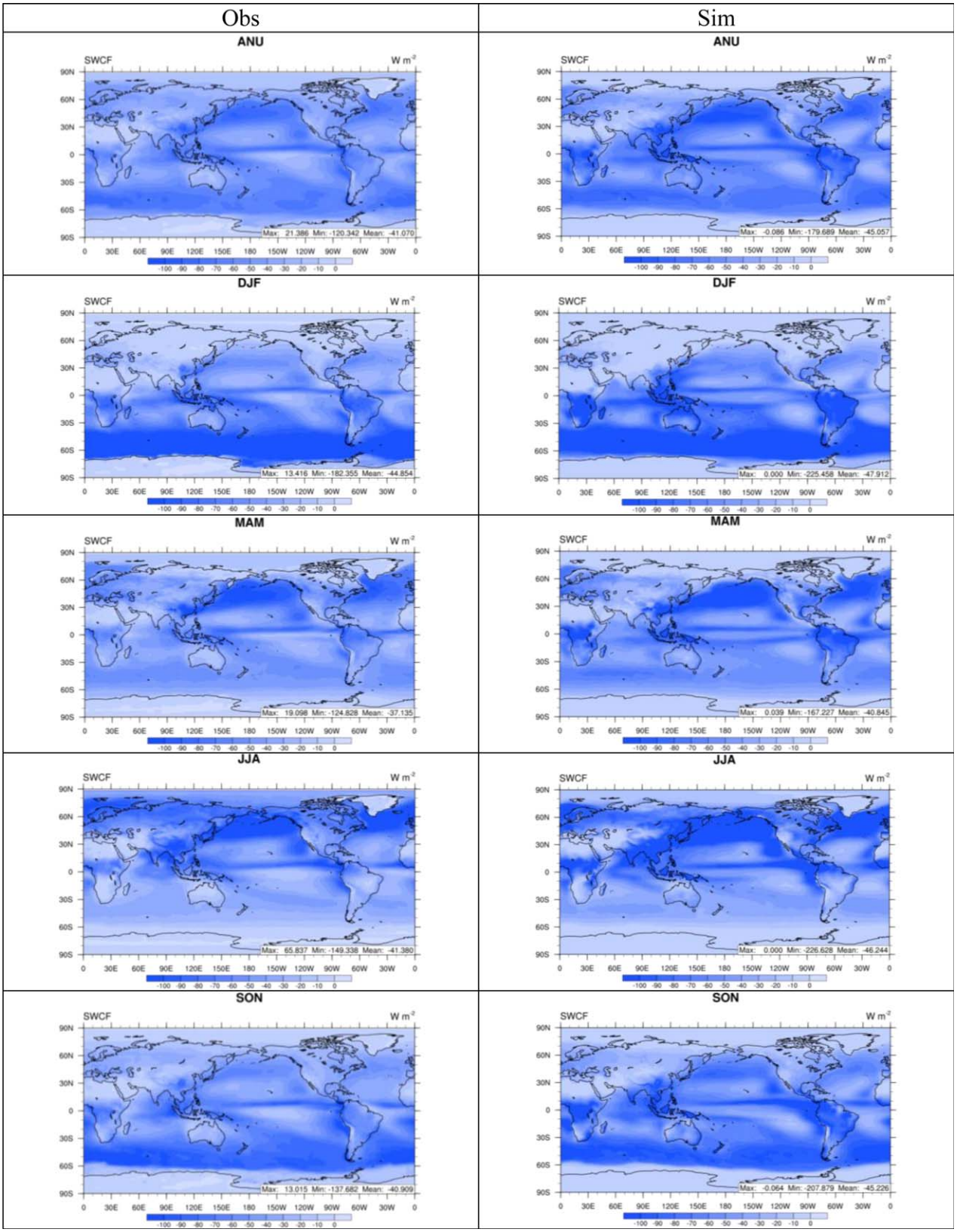

Figure 5. Seasonal and annual comparison of simulated SWCF (Sim.) against CERES observations (Obs.). From top to bottom: annual (ANU), December-January-February (DJF), March-April-May (MAM), June-July-August (JJA), and September-October-November (SON). The results are based on 10 year average of 2001–2010.

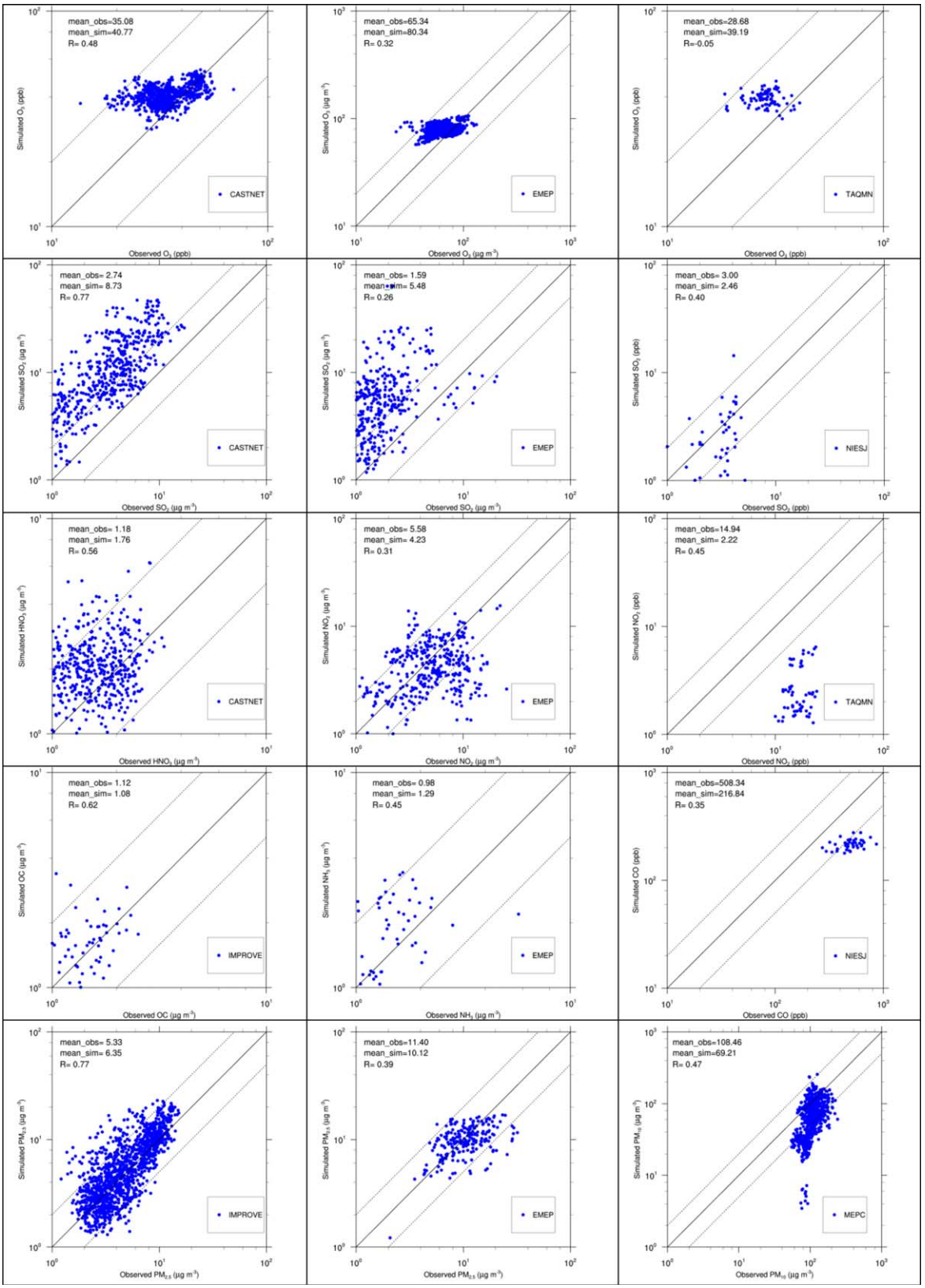

Figure 6. Scatterplots of major chemical species over various sites in different monitoring networks including CASTNET, IMPROVE, EMEP, MEPC, NIESJ, and TAQMN.

NO_2 concentrations are largely underpredicted over Europe, with an NMB of −77.7%, whereas NH_3 and HNO_3 concentrations are overpredicted over Europe, with NMBs of 31.9 and 41.8%, respectively. The biases of predictions in NH_3 and NO_2 concentrations could be due to the uncertainties in NH_3 and NO_x emissions. The overprediction of HNO_3 over Europe is likely due in part to overestimated oxidation of NO_2 resulted from overestimated OH concentrations, and/or underestimated dry deposition of HNO_3. FSNS is overpredicted over Europe (see Figure 1), allowing more photolytic reactions to produce OH (e.g., photolytic reactions of O_3 and VOCs), and therefore more OH can oxidize NO_2 to produce HNO_3. In addition, the observed surface OH concentrations vary from 0 to 6×10^6 molecules cm^{-3}, with a mean maximum value of 4.2×10^6 molecule cm^{-3} in summer over Europe [*Michoud et al*., 2012]. The summer (JJA) average of simulated OH over Europe is about 0.05–0.35 ppt (or $1–7 \times 10^6$ molecules cm^{-3}), indicating possible OH overpredictions. O_3 concentrations are predicted reasonably well over CONUS with an NMB of 16.2%, whereas they are largely overpredicted over Europe and East Asia, with NMBs of 47.8 and 48.5%, respectively. As shown in Figure 6, surface O_3 is overpredicted by 5.7 ppb (or by 16.2%) over the CASTNET sites, whereas it is overpredicted by 15 $\mu g\ m^{-3}$ (or by 23.0%) over the EMEP sites and overpredicted by 10.5 ppb (or by 36.6%) over the TAQMN sites. The overpredictions of O_3 over Europe and East Asia are likely due to the underprediction of O_3 titration resulting from the underprediction of NO_x. SO_4^{2-} concentrations are predicted reasonably well over CONUS and Europe, whereas NH_4^+ and NO_3^- concentrations are overpredicted over these regions, with NMBs of 37.4–59.8 to 44.8–93.2%. The overpredictions of HNO_3 concentrations over CONUS and Europe result in the overpredictions of NO_3^- concentrations over these regions. The overpredictions of NH_4^+ concentrations over CONUS and Europe are due possibly to the uncertainties in NH_3 emissions as well as overpredictions of HNO_3 over these regions, which can partition into NO_3^- to neutralize excess NH_4^+ through thermodynamic equilibrium. Cl^- concentrations are well predicted over CONUS but are largely overpredicted over Europe with an NMB of 376.0%, which is likely due to the uncertainties in the HCl and sea-salt emissions as well as treatments for coarse particulate chloride. The model only treats gas/particle equilibrium thermodynamics for fine inorganic particles and the condensation of major inorganic volatile gases (e.g., H_2SO_4, NH_3, HNO_3, and HCl) onto all aerosol modes is treated as irreversible, which can result in overpredictions of inorganic aerosol concentrations in the coarse mode, thus overpredictions of inorganic aerosol concentrations over all the modes (e.g., NH_4^+, NO_3^-, and Cl^- over Europe). The concentrations of OC, BC, and $PM_{2.5}$ are well predicted over CONUS, with absolute NMBs less than 16% whereas TC concentrations are underpredicted with an NMB of 37.9%. The discrepancy between OC/BC and TC performance is mainly due to the different observational data sets used for the evaluation. The OC observations are from IMPROVE, whereas BC and TC observations are from IMPROVE and STN. $PM_{2.5}$ and PM_{10} concentrations are moderately underpredicted over Europe and East Asia, with an NMB of −37.2 to −6.3%. As shown in Figure 6, the surface $PM_{2.5}$ concentration is underpredicted by 1.0 $\mu g\ m^{-3}$ (or by 16.1%) over the IMPROVE sites and underpredicted by 1.3 $\mu g\ m^{-3}$ (or by 11.2%) over the EMEP sites, whereas the surface PM_{10} concentration is underpredicted by 39.25 $\mu g\ m^{-3}$ (or by 36.2%) over the MEPC sites. The underpredictions of $PM_{2.5}/PM_{10}$ are likely due to the underpredictions of organic aerosol concentrations. The underpredictions of organic aerosol concentrations can be attributed in part to the uncertainties in the VOCs and OC emissions. Several studies indicated the uncertainties in the emission data used over CONUS, Europe, and Asia. For example, power plant and industry NO_x emissions over eastern U.S. have decreased by 50% between 1999 and 2003/2004 [*Frost et al*., 2006; *Hudman et al*., 2007]. It is not clear whether the U.S. National Emission Inventory has included such information. *Langmann et al*. [2008] suggested an updated emission by considering the changes in heating practices in Europe to improve the SOA predictions. The anthropogenic NO_x emissions over mainland China have increased from 3.8 TgN yr^{-1} in 2000 [*Zhang et al*., 2007] to 6.3 TgN yr^{-1} in 2006 [*Zhang et al*., 2009]. Emission inventories over all those regions, on the other hand, are not updated on a yearly basis. For example, the U.S. EPA updates the NEI every 3–4 years. In this work, emissions during 3 years, i.e., 2001, 2005, and 2008, are used to represent emissions for 2001–2010 based on the best available emissions from global and regional emission inventories. The lack of yearly varied emissions may lead to some inaccuracies in representing the emission interannual variations of the individual species, and therefore explaining some uncertainties in the model predictions. In *He and Zhang* [2014], a sensitivity simulation with emission adjustment was conducted to investigate the impacts of emissions on model predictions, which indicated that anthropogenic emissions on major chemical species, such as CO, SO_2, NO_2, NH_3, OC, and BC, have significant impacts on the model predictions. The underpredictions of organic aerosol concentrations may also be attributed in part to the uncertainties in the model treatments for SOA formation. The

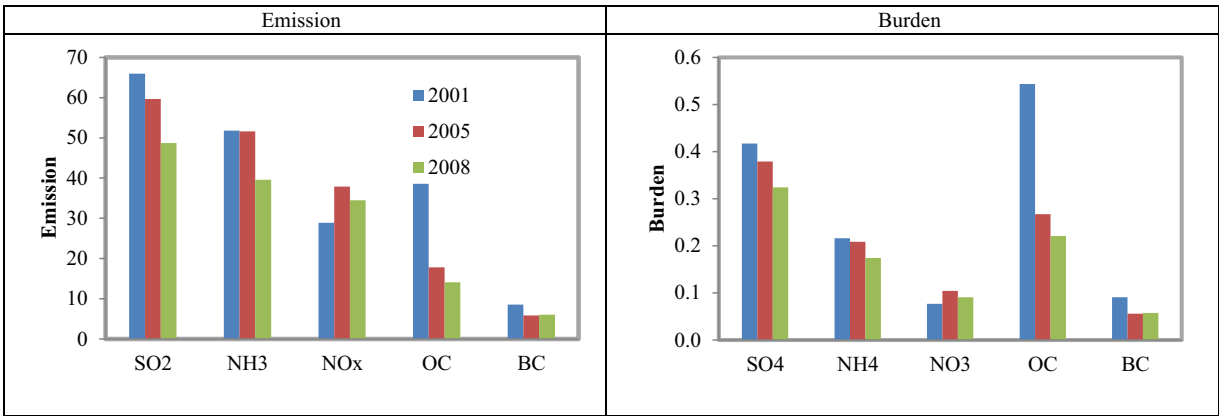

Figure 7. Emission trend and corresponding aerosol burden trend. Units for SO_2 emission and SO_4 burden are Tg S yr^{-1} and Tg S; units for NH_3 emission and NH_4 burden are Tg N yr^{-1} and Tg N; for NO_x emission and NO_3 burden are Tg N yr^{-1} and Tg N; units for OC/BC emissions and OC/BC burden are Tg yr^{-1} and Tg, respectively.

current VBS representation for SOA formation included in this work only includes biogenic VOCs and anthropogenic VOCs partitioning in both the gas and the condensed phases without consideration of SVOC and aging and volatility of POA. Including SVOC emissions and their subsequent oxidation has been shown to have a considerable impact on OC predictions over Europe [*Couvidat et al.*, 2012, 2013a]. Furthermore, the aqueous-phase oxidation of VOCs in clouds is not taken into account; although it is not a major SOA formation pathway, it can contribute several % in some areas and seasons over Europe [*Couvidat et al.*, 2013b].

The global tropospheric SO_2 column is underpredicted with NMB of −28.4%, which is likely due to uncertainties in SO_2 emissions. Tropospheric CO and NO_2 columns are largely overpredicted whereas surface concentrations of CO and NO_2 are underpredicted, suggesting the uncertainties in CO and NO_2 emissions in terms of spatial allocations as well as convective transport treatments. The global TOR is slightly underpredicted with an NMB of −3.5%. The global tropospheric HCHO column is largely underpredicted with an NMB of −44.6%, which is likely due partly to no biogenic HCHO emissions as well as uncertainties in biogenic isoprene emissions and its secondary HCHO formation. Figure 7 shows emission trends for SO_2, NH_3, NO_x, primary OC (POC), and BC. Emissions of SO_2, NH_3, and POC decrease from 2001 to 2008, whereas CO and NO_x emissions are higher in 2005 than 2001 and 2008, and BC emissions are lower in 2005 than 2001 and 2008. The corresponding aerosol burdens such as SO_4^{2-}, NH_4^+, NO_3^-, OC, and BC have strong correlations with the emission trends of SO_2, NH_3, NO_x, OC, and BC, respectively, due to the impacts of emissions on aerosol predictions. Meanwhile, other processes can affect chemical species predictions, such as kinetic reactions, condensation, and dry/wet deposition. For example, the reaction rate for oxidation of CO by OH is likely to decrease due to underpredictions of temperature, resulting in smaller loss of CO and OH and higher CO column concentrations. In addition, the uncertainties in the model treatments for dry and wet deposition can result in uncertainties in the removal of chemical species through those processes. For example, precipitation is underpredicted over 30°N–60°N, which can result in overpredictions of chemical concentrations in this region, whereas it is overpredicted over 30°S–30°N, which can result in underpredictions of chemical concentrations. The accommodation coefficients are usually measured under laboratory conditions; therefore, uncertainties may exist when they are extrapolated to ambient atmospheric conditions to simulate the formation of secondary aerosols through condensation of gaseous precursors under different atmospheric conditions and at the global scale.

4.1.3. Global Burden Analysis

Table 5 shows the simulated 10 year average global burdens of major gaseous and aerosol species for three emission periods. The global burdens of some gaseous species (e.g., tropospheric O_3, HCHO, NO_x, and NO_y, and total column of DMS, SO_2, and NH_3) are within 25% of differences comparing with previous studies, whereas there are large differences for other gaseous species such as CO, H_2SO_4, and HNO_3. Compared with the results of *He and Zhang* [2014], the 10 year mean global CO burden is about 105.5% higher but that of H_2SO_4 burden is about 69.5% lower in this work. The higher CO burden is likely due to the different kinetic reaction rate calculation for CO + OH used in this work, which is based on superfast chemistry in default CAM5. However, it turned out there was a typographical error in the rate constant for CO + OH in default

Table 5. Global Burdens of Major Gaseous and Aerosol Species (2001–2010)

	2001–2003	2004–2006	2007–2010	2001–2010	*He and Zhang* [2014]	Previous Studies
Tropospheric CO (Tg)[a]	712	726	576	661.87	322.06	337–354[c]
Tropospheric O_3 (DU)[a]	28.2	30.1	27.6	28.5	30.5	34.04[d]
Tropospheric O_3 (Tg)[a]	219.3	313.8	283.0	294.83	332.87	372[d]
DMS (Tg S)	0.073	0.064	0.065	0.067	0.058	0.067[e]
SO_2 (Tg S)	0.289	0.264	0.224	0.256	0.281	0.34[e]
H_2SO_4 (Tg S)	6.2×10^{-4}	5.7×10^{-4}	5.5×10^{-4}	5.8×10^{-4}	1.9×10^{-3}	4.2×10^{-4}[e]
Tropospheric NO_x[a,b] (molecules cm^{-2})	8.9×10^{14} (0.11 Tg N)	1.1×10^{15} (0.13 Tg N)	1.0×10^{15} (0.12 Tg N)	1.0×10^{15} (0.12 Tg N)	8.2×10^{14} (0.116 Tg N)	7.6×10^{14} to 9.2×10^{14}[f]
Tropospheric NO_y (Tg N)[b]	0.83	0.96	0.85	0.88	1.02	N.A.[g]
Tropospheric HNO_3 (Tg N)	0.11	0.13	0.12	0.12	0.12	0.5[c]
NH_3 (Tg N)	0.057	0.056	0.043	0.051	0.059	0.064[e]
VOCs (Tg C)[b]	7.14	5.97	5.89	6.29	7.63	N.A.[g]
Tropospheric HCHO (Tg C)[a]	0.340	0.321	0.293	0.315	0.391	0.335–0.349[c]
SO_4^{2-} (Tg S)	0.42	0.38	0.32	0.37	0.39	0.84[d], 0.47[e], 0.66[h]
NO_3^- (Tg N)	0.08	0.10	0.09	0.09	0.11	0.01–0.14[i]
NH_4^+ (Tg N)	0.22	0.21	0.17	0.20	0.21	0.24[e] (0.27–0.44)[i]
Na^+ (Tg)	3.82	3.82	3.85	3.83	3.04	2.98[d] (0.38–5.19)[i]
Cl^- (Tg)	5.64	5.64	5.68	5.66	4.47	4.60[d] (0.59–8.02)[i]
BC (Tg)	0.090	0.055	0.057	0.067	0.076	0.28[d], 0.093[e]
OC (Tg)	0.54	0.26	0.22	0.33	0.61	1.28[d]
POM (Tg)	0.63	0.25	0.20	0.35	0.48	0.68[e], 1.70[h]
SOA (Tg)	0.13	0.12	0.11	0.12	0.38	1.15[e], 0.59[j]
Dust (Tg)	27.2	29.0	26.4	27.4	26.4	24.7[e] (7.9–35.9)[i]

[a]Troposphere refers to model layers below tropopause height.

[b]$NO_x = NO + NO_2$; $NO_y = NO_x$ + nitrogen trioxide (NO_3) + dinitrogen pentoxide (N_2O_5) + nitrous acid (HONO) + nitric acid (HNO_3) + pernitric acid (HNO_4) + peroxyacyl nitrate (PAN) + d_3 peroxyacyl nitrate (PANX) + other organic nitrate (NTR); VOCs: volatile organic compounds, including acetaldehyde (ALD2), carboxylic acid (AACD), long-chain alkanes (ALKH), cresol and higher phenols (CRES), ethene (ETH), ethane (ETHA), ethanol (ETOH), formaldehyde (FORM), internal olefinic carbon bond (IOLE), methanol (MEOH), olefinic carbon bond (OLE), paraffin carbon bond (PAR), polycyclic aromatic hydrocarbons (PAH), toluene (TOL), xylene (XYL), isoprene (ISOP), and terpene (TERP).

[c]*Williams et al.* [2009].

[d]*Horowitz et al.* [2006].

[e]*Liu et al.* [2012].

[f]*Lamarque et al.* [2005].

[g]N.A.: not available. It refers to species having no burden data from previous studies.

[h]*Textor et al.* [2006].

[i]*Tsigaridis et al.* [2006].

[j]*Heald et al.* [2008].

CAM5 [see *Lamarque et al.*, 2013, supporting information], which could result in underprediction of CO loss from CO + OH and overprediction of CO burden. Precipitation, especially over 30°N–60°N (e.g., Europe and the middle/eastern U.S.), is underpredicted by 10–50%, resulting in low wet deposition. The reaction rate of oxidation CO by OH is affected by temperature and pressure. Temperature is underpredicted, decreasing the reaction rate of oxidation, which is likely to increase the CO burden. The lower H_2SO_4 burden is due to greater condensation of H_2SO_4 resulting from a larger mass accommodation coefficient of 0.1 compared to the value of 0.02 that was used by *He and Zhang* [2014]. However, compared with other studies, the H_2SO_4 burden is still relatively higher (e.g., a mass accommodation coefficient of 0.65 is used in *Liu et al.* [2012]), indicating the uncertainties in the H_2SO_4 condensation associated with its mass accommodation coefficient. The HNO_3 burden in this work is comparable with that from *He and Zhang* [2014], but it is about 76% lower than *Williams et al.* [2009]. The lower HNO_3 burden is likely due in part to the uncertainties in the NO_x emissions and overprediction of Precip in the low and middle latitudes.

As shown in Figure 7, chemical burdens are strongly correlated with emissions. In Table 4, the SO_4^{2-} and NH_4^+ burdens decrease during 2001–2010, whereas the NO_3^- burden increases from 2001–2003 to 2004–2006 and then decreases to 2007–2010. Most inorganic aerosol burdens are in the range of previous studies except those of SO_4^{2-} and NH_4^+. The SO_4^{2-} burden is slightly lower, which is likely due to the lower SO_2 emissions compared to the study of *Liu et al.* [2012] and missing SO_4^{2-} emissions. The lower SO_4^{2-} burden results in lower NH_4^+ burden. Compared with *Horowitz et al.* [2006], global burdens of BC and OC are lower by 76.1 and 59.4%, respectively. Compared with *Liu et al.* [2012], global burdens of BC, primary organic matter (POM), and SOA are lower by 28.5, 48.5, and 89.6%, respectively. The lower BC, OC, POM, and SOA burdens are likely due to uncertainties in the BC and OC emissions used in the model as well as differences in the

model treatments for SOA formation and POM aging. For example, *Liu et al*. [2012] used the default CAM5 SOA formation treatments, whereas the VBS representation of SOA formation is included in this work. Condensation onto the primary carbon mode produces aging of the particles in this mode. A lower accommodation coefficient is used in this work compared to *Liu et al*. [2012], resulting in less condensation. Therefore, the fraction of aged particles has decreased, which affects BC and POM concentrations.

4.1.4. Impacts of the Anthropogenic Emissions

To quantify the overall impacts of anthropogenic emissions on air quality and climate through atmospheric radiation and aerosol direct/indirect effects, anthropogenic emissions of both gaseous and PM species are reduced by 80% to represent the clean/background chemical conditions. Figures 8a–8c compare the CESM simulations with baseline emissions and with 20% of anthropogenic emissions from the baseline emissions. Primary aerosols such as BC and OC can be directly affected by the emissions. Secondary aerosols can be affected through chemical reactions and gas-particle partitioning. As shown in Figure 8a, with 80% higher anthropogenic emissions, the 10 year average domainwide-mean surface concentrations of SO_4^{2-}, SOA, and POM increase by 0.4 μg m^{-3} (or by 79.8%), 0.07 μg m^{-3} (or by 86.0%), and 0.23 μg m^{-3} (or by 81.4%), respectively. As a result, the surface concentrations of $PM_{2.5}$ and PM_{10} increase by 1.1 μg m^{-3} (or by 20.7%) and 1.5 μg m^{-3} (or by 6.1%) in the global mean. The smaller increase of PM_{10} compared to that of $PM_{2.5}$ is mainly due to the changes in online dust and sea-salt emissions through feedbacks from meteorology (e.g., WS10). Aerosol can be activated as CCN and therefore affect cloud properties. With 80% higher anthropogenic emissions, as shown in Figure 8b, domainwide-column CCN5, CDNC, and COT increase by 2.8 $\times$ 10^7 cm^{-2} (or by 52.7%), 39.3 cm^{-3} (or by 40.4%), and 1.6 (or by 14.7%) in the global mean. Due to more clouds from more aerosols, domainwide-SWCF increases by 3.2 W m^{-2} (or by 3.1%) in the global mean. Because of more reflection from aerosols and clouds, as shown in Figure 8c, FSDS decreases by 4.7 W m^{-2} (or by 2.9%), resulting in a domainwide-decrease in T2 by 1.0°C (or by 47.6%) in the global mean. WS10 is not affected significantly (figure not shown), but there is a 5% decrease in Precip in the global mean, PBLH is also affected, with increases as large as 101.6 m (or by 24.6%) or decreases as large as 169.2 m (or by 61.7%), and with a net decrease of 2.8 m (or by 0.8%) in the global mean.

4.2. Intercomparison of Simulations With Improved CESM/CAM5.1 and Simulations With CMIP5

Figure 9 shows the Taylor diagram [*Taylor*, 2001] comparing the model performance of CESM-NCSU with that of the CESM1-CAM5 output from CMIP5. The similarity between the two patterns is quantified in terms of their correlations (i.e., angle), their standard deviations (i.e., *y* axis), and the ratio of their variances (i.e., *x* axis). Compared with CESM-CMIP5, the bias of meteorological variables such as T2 and Q2 predicted by CESM-NCSU are larger whereas the bias of WS10 is similar and the bias of Precip is smaller. The larger biases of T2 and Q2 in CESM-NCSU are mainly due to the perturbations to the climate system resulting from higher aerosol concentrations as well as higher cloud predictions in CESM-NCSU. The bias of radiative variables from CESM-NCSU and CESM-CMIP5 are within the same range except for OLR, which shows a smaller bias in CESM-NCSU. The biases of CF, LWP, and AOD are smaller in CESM-NCSU than in CESM-CMIP5. The standardized deviations of most variables are lower in CESM-CMIP5 than in CESM-NCSU, especially for LWP and AOD. The lower standard deviation in CESM-CMIP5 is likely due to the lower variability from CESM-CMIP5 ensemble simulations. Compared with observations, the correlation coefficients for LWP and AOD are higher in CESM-NCSU than in CESM-CMIP5. The different model performance between CESM-NCSU and CESM-CMIP5 indicates the sensitivity of the climate system to perturbations in different model inputs (e.g., emissions) and model configurations (e.g., prescribed chemistry used in CESM-CMIP5 simulations), as well as the effect of the incorporation of new model treatments in CESM-NCSU.

Figure 10 compares zonal mean predictions from CESM-NCSU with CESM-CMIP5 against observations or reanalysis data. T2 and Q2 predicted by CESM-NCSU overall agree well with those by CESM-CMIP5, although T2 and Q2 from CESM-NCSU are lower than those from CESM-CMIP5 in tropical regions and the Northern Hemisphere. Compared with NCEP, the biases of T2 and Q2 from CESM-CMIP5 are smaller than those from CESM-NCSU. Precipitation predicted by CESM-NCSU overall agrees well with those predicted by CESM-CMIP5, although Precip from CESM-NCSU is lower than that from CESM-CMIP5 in 30°N–60°N. Compared with NCEP, the bias of Precip from CESM-CMIP5 is smaller than that from CESM-NCSU. Both CESM-NCSU and CESM-CMIP5 underpredict FSDS over tropical regions by 5–30 W m^{-2}. Compared with CERES observations, FLDS from CESM-NCSU is overall underpredicted (especially over higher latitudes in

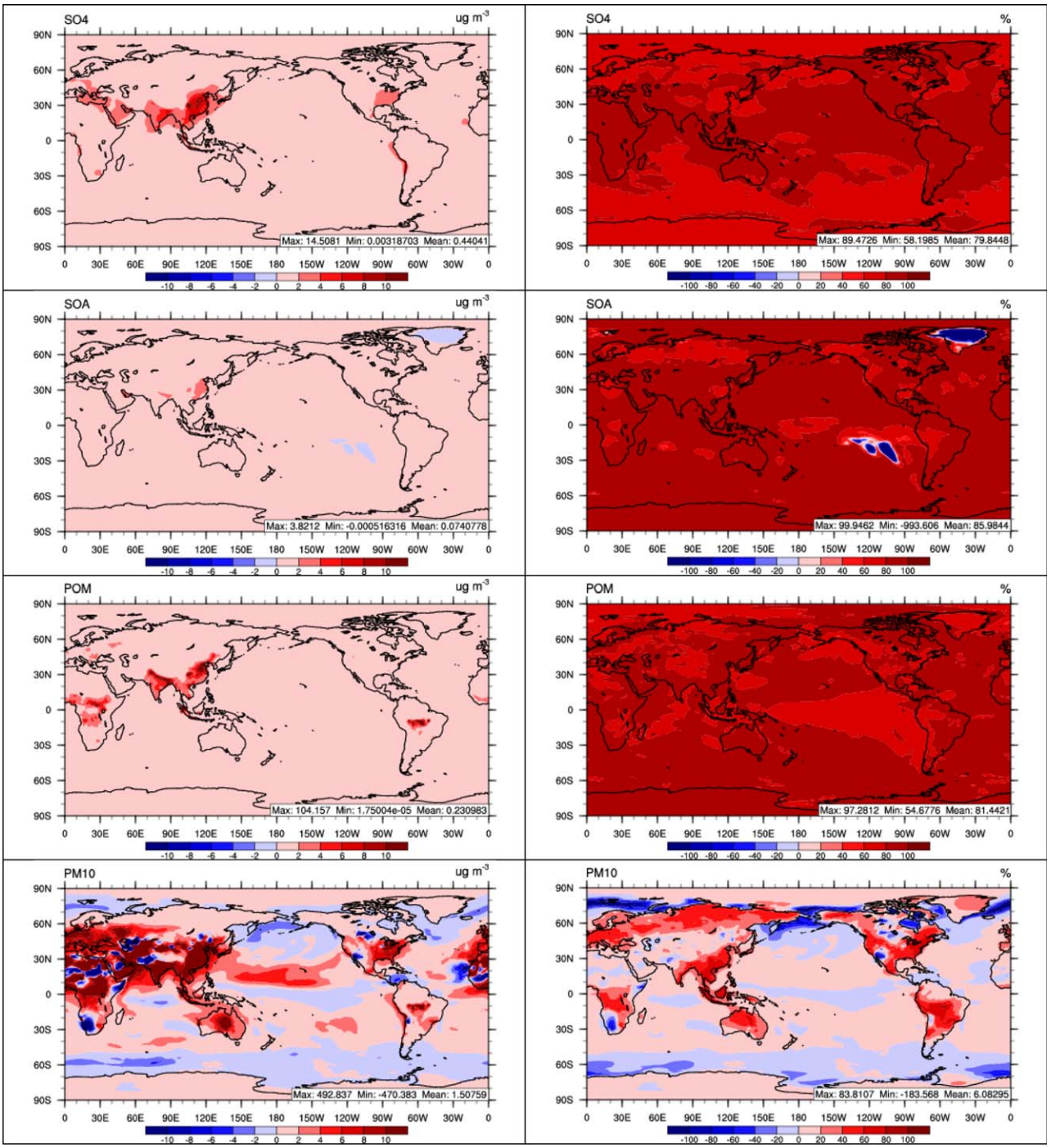

Figure 8. (a) Spatial distributions of absolute and percentage differences of sulfate (SO_4), SOA, POM, and PM_{10} between CESM simulations with baseline emissions and 20% of anthropogenic emissions from the baseline emissions. (b) Spatial distributions of absolute and percentage differences of CCN at s = 0.5%, CDNC, COT, and SWCF between CESM simulations with baseline emissions and 20% of anthropogenic emissions from the baseline emissions. (c) Spatial distributions of absolute and percentage differences of FSDS, T2, Precip, and PBLH between CESM simulations with baseline emissions and 20% of anthropogenic emissions from the baseline emissions.

the Southern Hemisphere and the entire Northern Hemisphere), whereas CESM-CMIP5 underpredicts FLDS mainly over higher latitudes in the Northern Hemisphere (figure not shown). The underpredictions of FLDS and FSDS result in the underprediction of T2. OLR from CESM-NCSU overall agrees well with that from CESM-CMIP5, although it is about 5–10 W m^{-2} lower in the Northern Hemisphere. Compared with NOAA/CDC observations, the bias of OLR (1.5 W m^{-2}) from CESM-NCSU is smaller than that from CESM-CMIP5 (5.8 W m^{-2}).

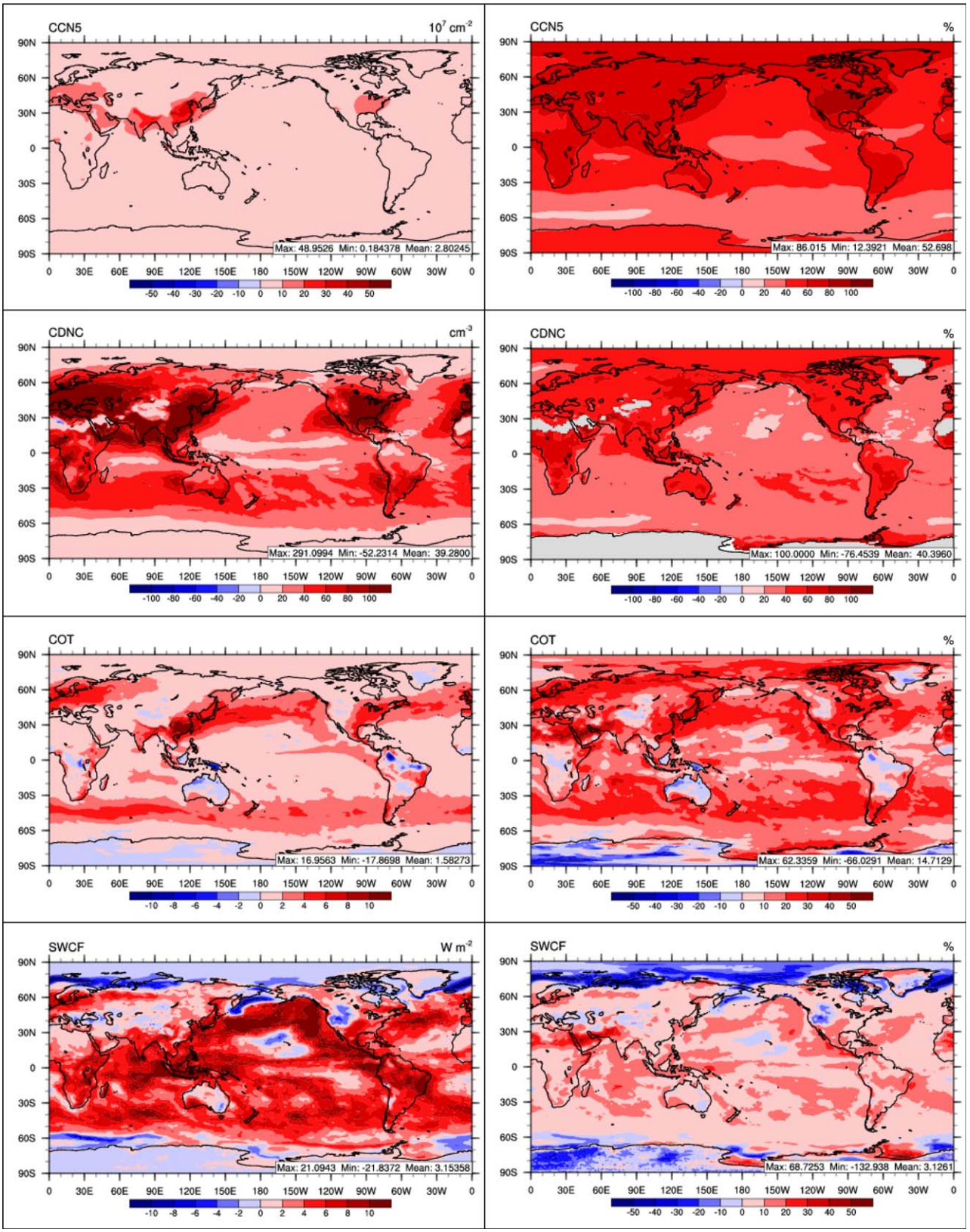

Figure 8. (continued)

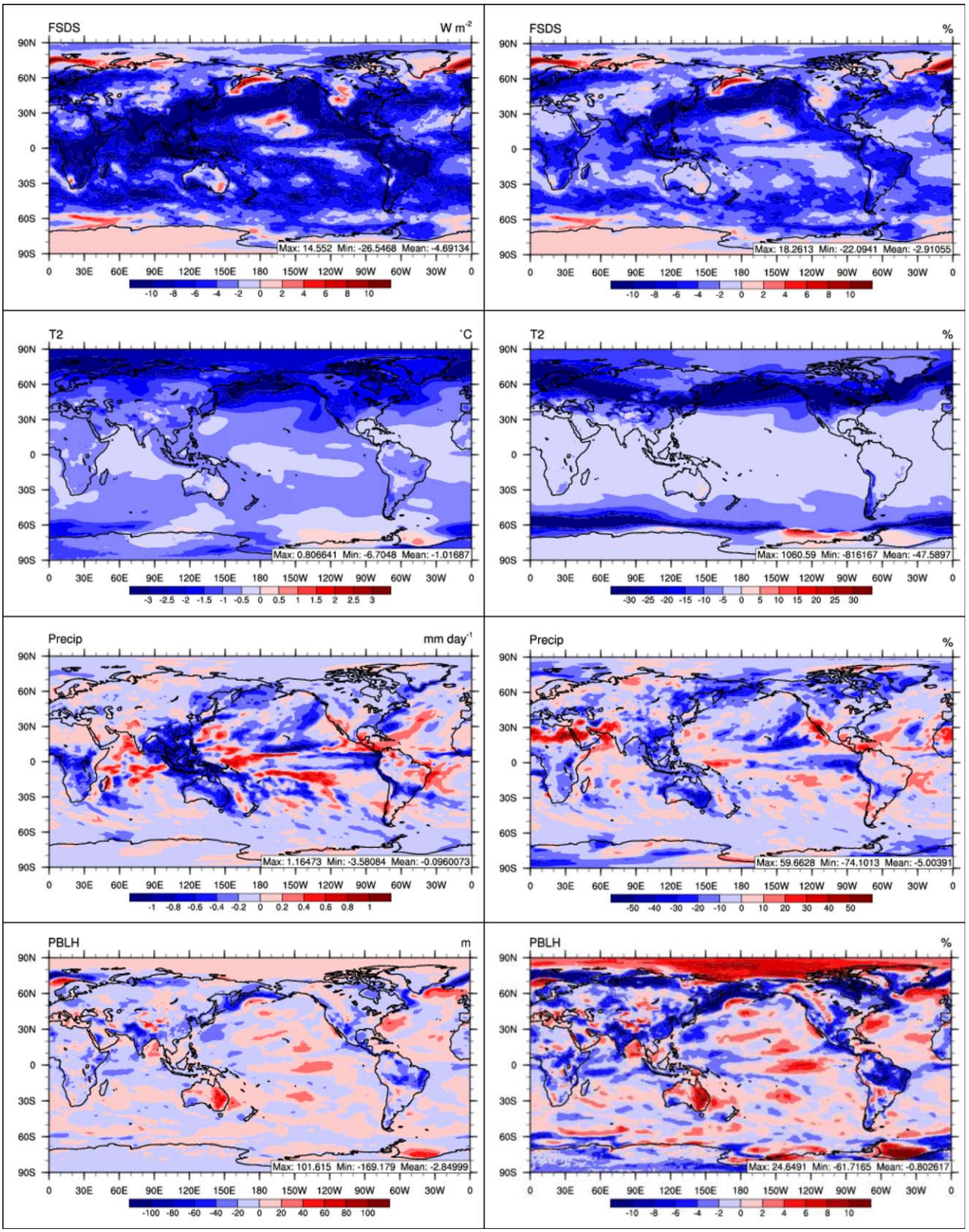

Figure 8. (continued)

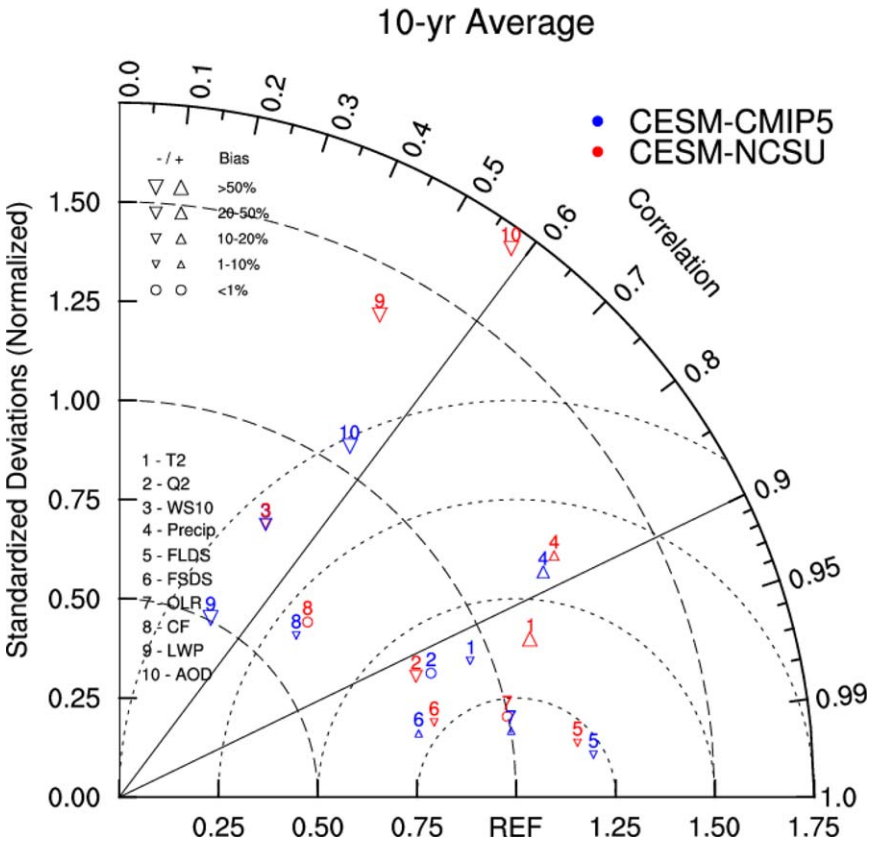

Figure 9. Taylor diagram of comparison between CESM-NCSU and CESM-CMIP5. The results are based on 10 year average. This diagram represents the similarity between CESM-NCSU and CESM-CMIP5. *X*-axis represents the ratio of variances between observations and simulations (proportional to the reference point identified as "REF"), and *Y*-axis represents the normalized standard deviation between the two patterns (proportional to the radial distance from the origin).

CF from CESM-NCSU agrees well with that from CESM-CMIP5, although it is higher in Northern Hemisphere, especially over the North Pole. Compared with MODIS data, CF from CESM-NCSU and CESM-CMIP5 are lower over low midlatitudes whereas they are higher over the polar regions. AOD predicted by CESM-NCSU is higher over 10°N–40°N but agrees better with satellite observations than CESM-CMIP5, due in part to higher dust concentrations in CESM-NCSU. However, AOD is still underpredicted especially over 50°S–90°S and 40°N–90°N. The underprediction of AOD can be due to the uncertainties in the optical properties and uncertainties in predictions of aerosol concentrations as well in the retrievals of oceanic AOD from MODIS data. The aerosol optical properties are defined for each mode of the MAM as described by *Ghan and Zaveri* [2007]. Hygroscopicity characteristics are specified for soluble species. For each shortwave band calculation, aerosol extinction, single scattering albedo, and asymmetry parameter are specified. For each longwave band, mass-specific absorption is specified. These optical properties are species-dependent. Composition of organic aerosol and soil dust is highly complex and variable, resulting in uncertainties in their optical properties. All such uncertainties can contribute to the uncertainty in AOD predictions. While simulated and observed SWCF agree reasonably well, large discrepancies exist between observed CDNC, COT, and LWP and simulated values from CESM_NCSU, in particular, in the polar regions. This can be attributed in part to the bias in these variables from MODIS at high latitudes and model's limitation in simulating cloud-related treatments.

Figure 11 shows the comparison of spatial distributions of T2, Precip, AOD, and FSDS from observations, CESM-CMIP5, and CESM-NCSU. Compared with NCEP/NCAR reanalysis data, T2 from CESM-CMIP5 agrees better than that from CESM-NCSU, especially over the tropical ocean (e.g., tropical Indian Ocean and tropical Pacific Ocean). T2 from CESM-NCSU is underpredicted (<2°C) over these regions, which is due to the underpredictions of SST. The underprediction of SST is due partly to the underprediction of FSDS as well as the uncertainties in the ocean initial conditions. Precip from CESM-CMIP5 and CESM-NCSU agree well with that

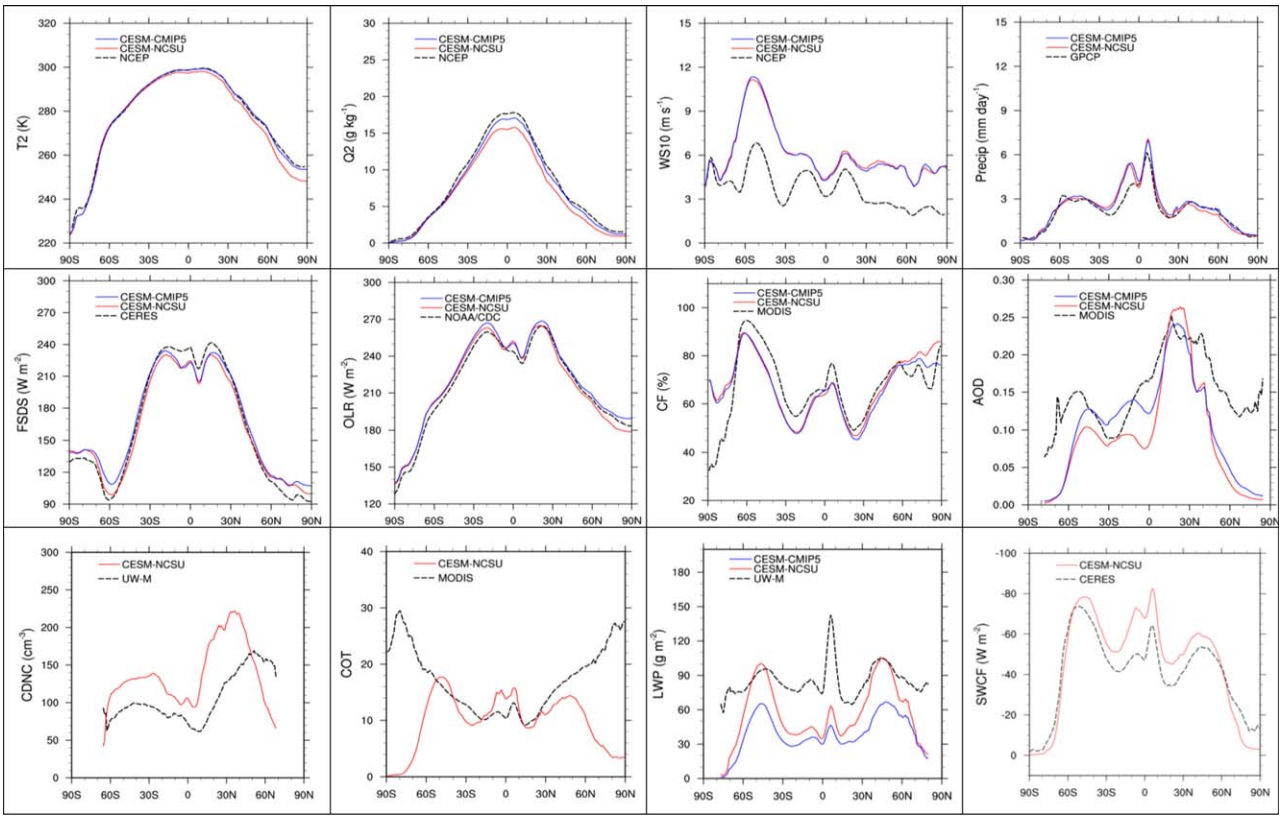

Figure 10. Comparison of 10 year average zonal mean predictions from CESM-NCSU and CESM-CMIP5 with observations/reanalysis data.

from GPCP. However, both CESM-CMIP5 and CESM-NCSU overpredict the Intertropical Convergence Zone (ITCZ) in the Northern Hemisphere and predict another ITCZ around 5°S–15°S. The double ITCZ has been identified as a systematic error in most climate models, including those CMIP5 models. FSDS from CESM-CMIP5 and CESM-NCSU agree well with that from CERES. However, both CESM-CMIP5 and CESM-NCSU underpredict FSDS by 5–10 W m^{-2} over the tropical oceans, which is likely due to the overprediction of CDNC over these regions. Both CESM-CMIP5 and CESM-NCSU capture hot spots for observed AOD over the Sahara and the Mediterranean Sea, whereas CESM-CMIP5 failed to predict AOD over East Asia and CESM-NCSU largely underpredicted AOD over most oceanic areas. The large underprediction of AOD is mainly due to the inaccurate predictions of aerosol concentrations.

5. Interannual Variability

Figure 12a shows the time evolution along with interannual variations of tropospheric column mass abundances of ozone, NO_2, HCHO, and $PM_{2.5}/PM_{10}$ over AUS, NAM, SAF, SAM, and SEA, and Figure 12b shows similar plots for AOD, column CCN5, CDNC, and SWCF over the same five regions. The model in general can capture the interannual variations of tropospheric ozone column and NO_2, column with some exceptions (e.g., TOR over SAF and SAM, and column NO_2 over AUS and NAM). Compared with TOMS/SBUV and OMI/MLS data, the tropospheric ozone column is relatively well predicted over AUS, where it is slightly overpredicted over NAM and SEA and largely underpredicted over SAF and SAM. The correlation between simulated and observed time evolution of TOR is relatively well over AUS and SEA. The TOMS/SBUV and OMI/MLS data show decreases of TOR during 2001–2010 over NAM and SEA indicated, however, the model fails to predict the decreasing trend over NAM but captures the decreasing trend over SEA. Compared with the SCIAMACHY data, the tropospheric NO_2 column is slightly overpredicted over SAM and SEA and largely overpredicted over AUS and NAM. The tropospheric NO_2 column is much higher over SEA than other regions, which is mainly due to the higher NO_x emissions over this region. The correlation of simulated and

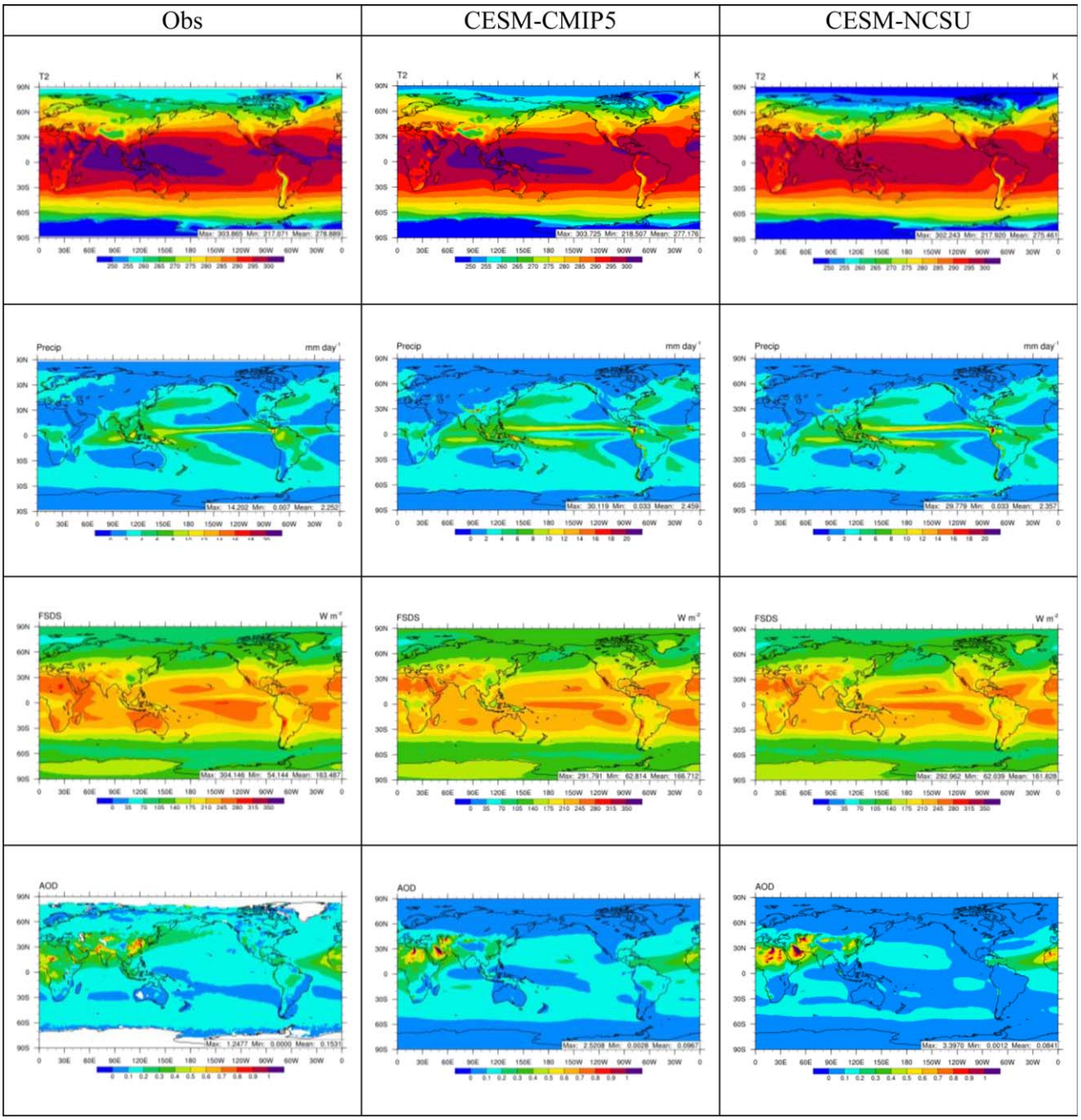

Figure 11. Comparison of 10 year average spatial distributions of T2, Precip, FSDS, and AOD from (left column) observations, (middle column) CESM-CMIP5, and (right column) CESM-NCSU.

observed time evolution of tropospheric NO_2 column is relatively good over SAF, SAM, and SEA. The SCIAMACHY data indicate an increasing trend of tropospheric NO_2 over SEA during 2001–2010, which is also captured in the model. Compared with the GOME and SCIAMACHY data, the correlation of simulated and observed time evolution of tropospheric HCHO column is relatively poor over AUS, NAM, SAF, and SAM. The HCHO column increases over AUS, SAF, and SAM during 2001–2010, but the model fails to capture this trend. While the model can capture interannual variations of tropospheric HCHO column in terms of the annual crests over SEA, it largely underpredicts the annual troughs. The model largely underpredicts tropospheric HCHO column over all five regions, which is mainly due to the uncertainties in the emissions of HCHO and its precursors (e.g., biogenic emissions) as well as HCHO retrievals.

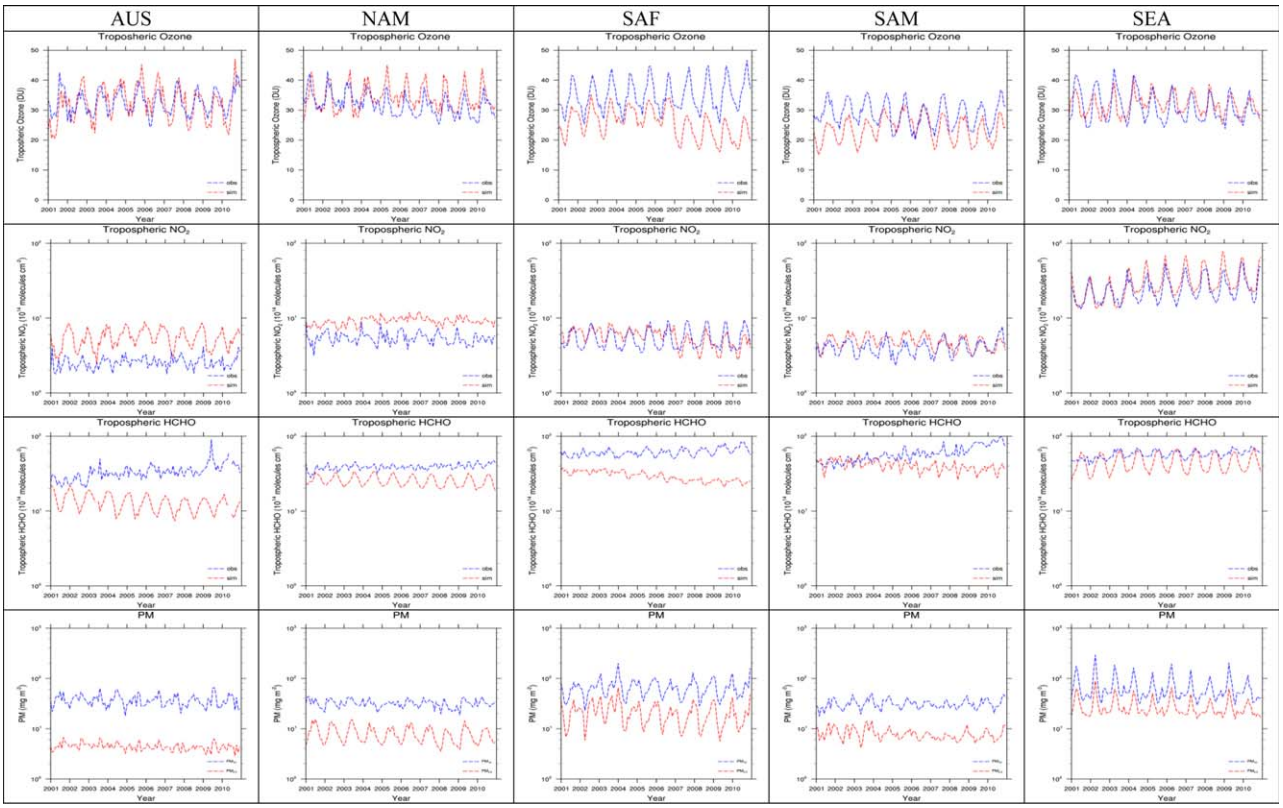

Figure 12. (a)Time series of 10 year (2001–2010) average observed and simulated tropospheric column mass abundances of O_3, NO_2, and SO_2, and simulated column concentrations of $PM_{2.5}$ and PM_{10} (note that no observations for column $PM_{2.5}$ or PM_{10} concentrations) over AUS, NAM, SAF, SAM, and SEA. (b) Time series of 10 year (2001–2010) average observed and simulated AOD, column CCN5, CDNC, and SWCF over AUS, NAM, SAF, SAM, and SEA.

The $PM_{2.5}/PM_{10}$ burdens over SAF and SEA are higher than those over AUS, NAM, and SAM, with mean concentrations of 21.3/66.8 and 27.7/67.5 mg m^{-2}, respectively. The higher PM burden with mass fraction of coarse particles of 68.1% over SAF is mainly due to the dust emissions, whereas the higher PM burden with a mass fraction of coarse particles of 59.0% over SEA is due partly to the emissions of dust, sea salt, and higher anthropogenic emissions. The higher mass fraction of coarse particles over AUS, NAM, and SAM are mainly from sea salt over oceanic areas. Higher PM burdens result in higher AOD and column CCN5.

The interannual variations of PM, column CCN5, and AOD over AUS, NAM, and SAM are not as strong as those over SAF and SEA. The variability of $PM_{2.5}/PM_{10}$ is larger over SAF and SEA than AUS, NAM, and SAM, with standard deviations (SD) of 3.4/6.7 and 3.1/9.6, respectively. Variation of AOD and column CCN5 over SAF and SEA correlates strongly with PM, whereas CDNC does not always correlate with PM, which is likely due to the impacts from other processes such as droplet nucleation, evaporation, and precipitation. Compared with MODIS data, the model can capture the interannual variations of AOD and CCN5, although the model underpredicts the magnitudes of AOD and CCN5 over most regions. The underpredictions of AOD over SAF and SEA are mainly due to the uncertainties in the model treatment of dust emissions. The underpredictions of CCN5 are mainly due to the underpredictions of PM as well as uncertainties in the cloud microphysics. Compared with the MODIS-derived CDNC data, the model in general can capture the interannual variations of CDNC; however, it largely overpredicts CDNC over all five regions. The overpredictions of CDNC are mainly due to the uncertainties in the model treatment (e.g., aerosol activation and cloud microphysics) as well as satellite data retrieval that have been discussed previously. Compared with the CERES data, the model can capture the interannual variation of SWCF very well over all five regions, although it slightly-to-moderately overpredicts SWCF over NAM and SEA. The variability of SWCF is larger over AUS and NAM than SAF, SAM, and SEA, with SD of 4.7 and 5.5, respectively, whereas the mean SWCF is higher in NAM, SAM, and SEA, with regional mean of -75.5, -72.2, and -78.4 W m^{-2}, respectively. The variability of SWCF does not necessarily correlate with CDNC, which is mainly due to impacts from other cloud variables such as COT.

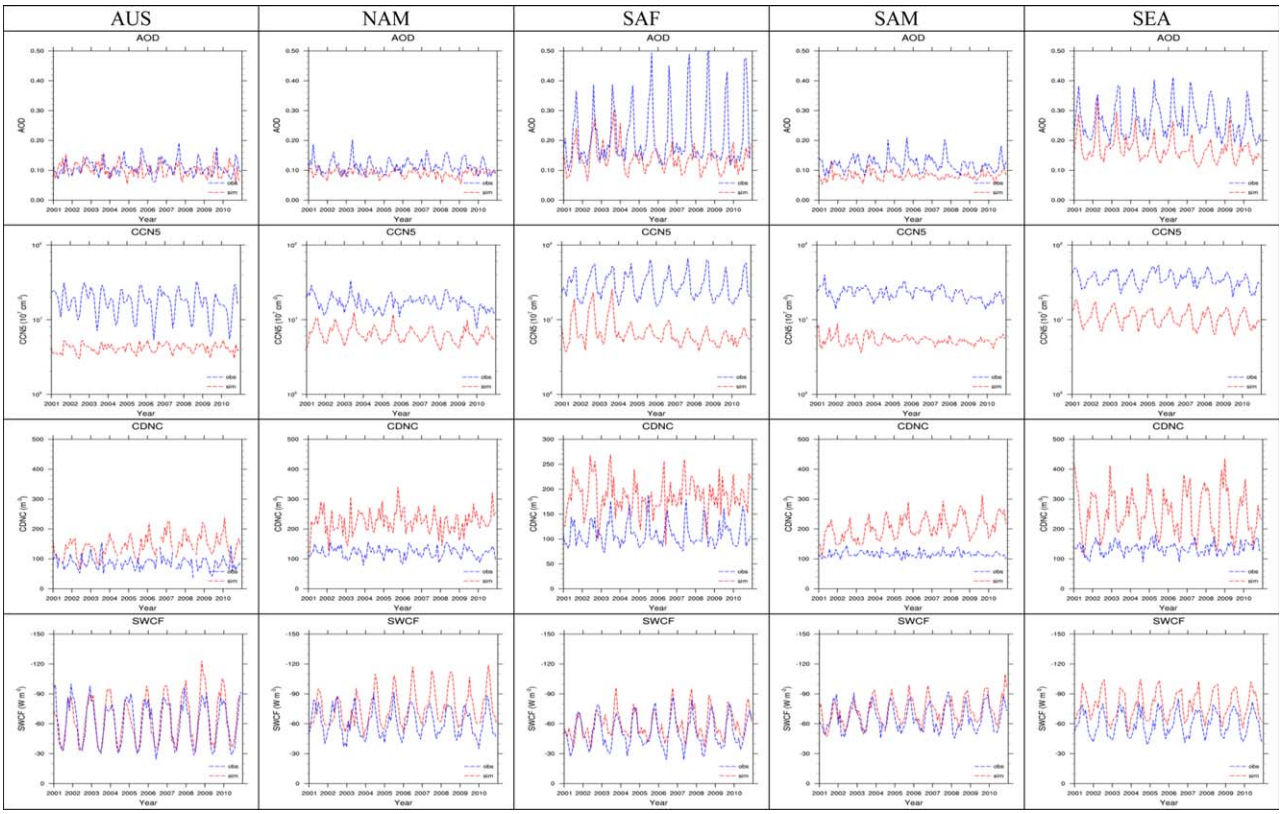

Figure 12. (continued)

6. Conclusions

In this work, a comprehensive evaluation has been conducted through applying CESM/CAM5.1 with advanced chemistry-aerosol-cloud interactions treatments for retrospective decadal simulations during 2001–2010. Meteorological and radiative variables are overall well predicted with NMBs of −14.1 to −9.7% and 0.7–10.8%, respectively, except T2, which is underpredicted by 22.2% compared to NCDC and 45.1% compared to NCEP/NCAR reanalysis data. CF and PWV are well predicted, with NMBs of −10.5 to 0.4%, whereas CCN, LWP, and COT are moderately-to-largely underpredicted, with NMBs of −82.2 to −31.2%, and CDNC is overpredicted by 26.7%, suggesting the uncertainties in the model treatments for cloud microphysics (e.g., resolved and subgrid-scale cumulus clouds) and/or satellite retrieval algorithms (e.g., error propagations in deriving cloud variables and plane-parallel visible-near-infrared retrievals with low solar zenith angle).

Concentrations of SO_4^{2-}, Cl^-, OC, and $PM_{2.5}$ are relatively well predicted over CONUS with NMBs of −12.8 to −1.18%, whereas O_3 concentrations over CONUS are slightly overpredicted with an NMB of 16.2% and BC concentrations are slightly underpredicted with an NMB of −15.6%. Surface O_3 mixing ratios (or concentrations) are overpredicted by 5.7 ppb (or by 16.2%) over the CASTNET sites, by 15 μg m^{-3} (or by 23.0%) over the EMEP sites, and by 10.5 ppb (or by 36.6%) over the TAQMN sites. Concentrations of SO_2, SO_4^{2-}, and PM_{10} are relatively well predicted over Europe with NMBs of −20.8 to −5.2%. The surface $PM_{2.5}$ concentrations are underpredicted by 1.0 μg m^{-3} (or by 16.1%) over the IMPROVE sites and by 1.3 μg m^{-3} (or by 11.2%) over the EMEP sites, and the surface $PM_{10.5}$ concentrations are underpredicted by 39.25 μg m^{-3} (or by 36.2%) over the MEPC sites. SO_2 concentrations are relatively well predicted over East Asia with an NMB of −18.2%. TOR is well predicted over the globe with an NMB of −3.5%. Large biases for some chemical predictions can be attributed to uncertainties in the emissions and model treatments. For example, SO_2 concentrations over CONUS are largely overpredicted, which is likely due to uncertainties in the SO_2 emissions and measurements, as well as less SO_2 wet deposition from underpredictions of Precip. SO_2 and PM_{10} over East Asia are underpredicted, which is likely due to uncertainties in the emissions of SO_2, PM

constituents (e.g., POC, dust, and sea salt) as well as other PM precursors. O_3 concentrations are overpredicted over Europe and East Asia, likely due to the underprediction of O_3 titration, resulting from underprediction of NO_x concentrations. The model only treats thermodynamics for fine inorganic particles and condensation is treated irreversible, which can result in overpredictions of inorganic aerosol concentration in coarse modes, and therefore inorganic aerosol concentrations over all the modes (e.g., NH_4^+, NO_3^-, and Cl^- over Europe). OC is typically underpredicted. Uncertainties in emissions of SVOCs could be a major cause of those underpredictions. Comparisons of the CESM simulation with baseline emissions and 80% reduced anthropogenic emissions indicate the significant impacts of anthropogenic emissions on radiation and climate predictions. With 80% higher anthropogenic emissions, FSDS can decrease by 4.7 W m^{-2} (or by 2.9%) domainwide-mean and as large as 14.6 W m^{-2} (or by 18.3%), and SWCF can increase by 3.2 W m^{-2} (or by 3.1%) in the global mean, and as large as 21.1 W m^{-2} (or by 68.7%). These results indicate the important role of anthropogenic emissions in the climate system and a need to develop co-benefited emission control strategies for air pollution control and climate mitigation.

Most meteorological and radiative variables predicted by CESM-NCSU overall agree well with those by CESM-CMIP5, although the bias of T2 from CESM-NCSU is larger than that from CESM-CMIP5. AOD predicted by CESM-NCSU is higher but agrees better with satellite observations than AOD from CESM-CMIP5, due in part to higher dust concentrations in CESM-NCSU. Model inputs (e.g., emissions and ocean initial conditions), model configurations as well as model treatments differ between CESM-NCSU and CESM-CMIP5; these differences can result in different perturbations in the climate system, and thus different meteorology and radiation predictions.

The model can generally predict the interannual variations of major chemical species, such as tropospheric O_3 column and tropospheric NO_2 column with some exceptions (e.g., tropospheric O_3 over SAF and SAM, and NO_2 over AUS and NAM). The correlation of time series of tropospheric O_3 is relatively well over AUS and SEA, and the model can capture the decreasing trend of tropospheric O_3 over SEA during 2001–2010. The correlation of time series of tropospheric NO_2 column is relatively good over SAF, SAM, and SEA, and the model can capture the increasing trend of tropospheric NO_2 over SEA during 2001–2010. The correlation of time series of tropospheric HCHO column is relatively poor over AUS, NAM, SAF, and SAM, and tropospheric HCHO column is largely underpredicted over the five regions. The interannual variations of PM, column CCN5, and AOD indicate the strong correlation of CCN and AOD with PM. CDNC does not always correlate with PM, due to the impacts from other processes such as droplet nucleation, evaporation, and precipitation. Likewise, SWCF does not always correlate with CDNC, due to the impacts from other cloud variables such as COT.

Comparing to CESM-CMIP5, the results from the 2001–2010 decadal simulations of CESM with advanced chemistry/aerosol treatment can provide a more accurate description of the interactions among chemistry, aerosol, and climate in the current atmosphere. It will therefore be a promising model for current and future decadal climate simulations under various emission scenarios to project climate change with reduced uncertainties associated with such interactions.

Acknowledgments

This work was sponsored by the U.S. National Science Foundation EaSM program AGS-1049200. The authors would like to thank Brett Gantt and Xin Zhang, former members of Air Quality Forecasting Lab, NCSU, for implementing advanced aerosol activation scheme into CAM5.1. Thanks are due to Christian Seigneur, CEREA, for his comprehensive and careful review of a draft of this manuscript. MODIS data and CERES data are provided by NASA via http://ladsweb.nascom.nasa.gov/data/search.html and http://ceres.larc.nasa.gov/order_data.php, respectively. Other surface network data were downloaded from their respective web sites. We would like to acknowledge high-performance computing support from Yellowstone (ark:/85065/d7wd3xhc) provided by NCAR's Computational and Information Systems Laboratory, sponsored by the U.S. National Science Foundation. AQMEII emissions for CONUS are prepared by U.S. EPA, Environment Canada, Mexican Secretariat of the Environment and Natural Resources, and National Institute of Ecology. AQMEII emissions for Europe are provided by Alessandra Balzarini, Research on Energy System (RES), Italy. MEIC emissions for China are provided by Qiang Zhang, Tsinghua University, China. For simulation results presented in this paper, please contact the corresponding author.

References

Abdul-Razzak, H., and S. J. Ghan (2000), A parameterization of aerosol activation: 2. Multiple aerosol types, *J. Geophys. Res.*, *105*(D5), 6837–6844, doi:10.1029/1999JD901161.

Ahmadov, R., et al. (2012), A volatility basis set model for summertime secondary organic aerosols over the eastern United States in 2006, *J. Geophys. Res.*, *117*, D06301, doi:10.1029/2011JD016831.

Andreae, M. O. (2009), A new look at aging aerosols, *Science*, *326*, 1493–1494, doi:10.1126/science.1183158.

Barahona, D., R. E. L. West, P. Stier, S. Romakkaniemi, H. Kokkola, and A. Nenes (2010), Comprehensively accounting for the effect of giant CCN in cloud activation parameterizations, *Atmos. Chem. Phys.*, *10*(5), 2467–2473, doi:10.5194/acp-10-2467-2010.

Barth, M. C., P. J. Rasch, J. T. Kiehl, C. M. Benkovitz, and S. E. Schwartz (2000), Sulfur chemistry in the National Center for Atmospheric Research Community Climate Model: Description, evaluation, features and sensitivity to aqueous chemistry, *J. Geophys. Res.*, *105*(D1), 1387–1415.

Bellouin, N., J. Rae, A. Jones, C. Johnson, J. Haywood, and O. Boucher (2011), Aerosol forcing in the Climate Model Intercomparison Project (CMIP5) simulations by HadGEM2-ES and the role of ammonium nitrate, *J. Geophys. Res.*, *116*, D20206, doi:10.1029/2011JD016074.

Bennartz, R. (2007), Global assessment of marine boundary layer cloud droplet number concentration from satellite, *J. Geophys. Res.*, *112*, D02201, doi:10.1029/2006JD007547.

Bretherton, C. S., and S. Park (2009), A new moist turbulence parameterization in the community atmosphere model, *J. Clim.*, *22*, 3422–3448.

Chuang, P. Y. (2003), Measurement of the timescale of hygroscopic growth for atmospheric aerosols, *J. Geophys. Res.*, *108*(D9), 4282, doi:10.1029/2002JD002757.

Collins, W. D., et al. (2004), Description of the NCAR Community Atmosphere Model (CAM 3.0), *NCAR Tech. Note NCAR/TN-464+STR*, Natl. Cent. for Atmos. Res., Boulder, Colo.

Collins, W. J., et al. (2011), Development and evaluation of an Earth-System model—HadGEM2, *Geosci. Model Dev.*, *4*, 1051–1075.

Couvidat, F., É. Debry, K. Sartelet, and C. Seigneur (2012), A hydrophilic/hydrophobic organic (H_2O) model: Development, evaluation and sensitivity analysis, *J. Geophys. Res.*, *117*, D10304, doi:10.1029/2011JD017214.

Couvidat, F., K. Sartelet, and C. Seigneur (2013a), Investigating the impact of aqueous-phase chemistry and wet deposition on organic aerosol formation using a molecular surrogate modeling approach, *Environ. Sci. Technol.*, *47*, 914–922.

Couvidat, F., Y. Kim, K. Sartelet, C. Seigneur, N. Marchand, and J. Sciare (2013b), Modeling secondary organic aerosol in an urban area: Application to Paris, France, *Atmos. Chem. Phys.*, *13*, 983–996.

Donahue, N. M., A. L. Robinson, C. O. Stanier, and S. N. Pandis (2006), Coupled partitioning, dilution, and chemical aging of semivolatile organics, *Environ. Sci. Technol.*, *40*, 2635–2643.

Donahue, N. M., S. A. Epstein, S. N. Pandis, and A. L. Robinson (2011), A two-dimensional volatility basis set: 1. Organic-aerosol mixing thermodynamics, *Atmos. Chem. Phys.*, *11*, 3303–3318.

Donahue, N. M., J. H. Kroll, S. N. Pandis, and A. L. Robinson (2012), A two-dimensional volatility basis set: 2. Diagnostics of organic-aerosol evolution, *Atmos. Chem. Phys.*, *11*, 615–634.

Dunne, J. P., et al. (2012), GFDL's ESM2 global coupled climate-carbon earth system models. Part I: Physical formulation and baseline simulation characteristics, *J. Clim.*, *25*, 6646–6665.

Dunne, J. P., et al. (2013), GFDL's ESM2 global coupled climate-carbon earth system models. Part II: Carbon system formulation and baseline simulation characteristics, *J. Clim.*, *26*, 2247–2267.

Dutkiewicz, S., A. P. Sokolov, J. Scott, and P. H. Stone (2005), A three-dimensional ocean-seaice-carbon cycle model and its coupling to a two-dimensional atmospheric model: Uses in climate change studies, *MIT JPSPGC Rep. 122*, 47 p., MIT Joint Program on the Sci. and Policy of Global Change, Cambridge, Mass.

Emmons, L. K., et al. (2010), Description and evaluation of the model for ozone and related chemical tracers, version 4 (MOZART-4), *Geosci. Model Dev.*, *3*, 43–67, doi:10.5194/gmd-3-43-2010.

Fountoukis, C., and A. Nenes (2005), Continued development of a cloud droplet formation parameterization for global climate models, *J. Geophys. Res.*, *110*, D11212, doi:10.1029/2004JD005591.

Fountoukis, C., and A. Nenes (2007), ISORROPIA II: A computationally efficient thermodynamic equilibrium model for K^+-Ca^{2+}-Mg^{2+}-NH_4^+-Na^+-SO_4^{2-}-NO_3^--Cl^--H_2O aerosols, *Atmos. Chem. Phys.*, *7*, 4639–4659, doi:10.5194/acp-7-4639-2007.

Frost, G. J., et al. (2006), Effects of changing power plant NO_x emissions on ozone in the eastern United States: Proof of concept, *J. Geophys. Res.*, *111*, D12306, doi:10.1029/2005JD006354.

Gantt, B., J. He, X. Zhang, Y. Zhang, and A. Nenes (2014), Incorporation of advanced aerosol activation treatments into CESM/CAM5: Model evaluation and impacts on aerosol indirect effects, *Atmos. Chem. Phys.*, *14*, 7485–7497.

GFDL Global Atmospheric Model Development Team (2004), The new GFDL Global Atmosphere and Land Model AM2-LM2: Evaluation with prescribed SST simulations, *J. Clim.*, *17*, 4641–4673.

Ghan, S. J., and R. A. Zaveri (2007), Parameterization of optical properties for hydrated internally mixed aerosol, *J. Geophys. Res.*, *112*, D10201, doi:10.1029/2006JD007927.

Ghan, S. J., H. Abdul-Razzak, A. Nenes, Y. Ming, X. Liu, M. Ovchinnikov, B. Shipway, N. Meskhidze, J. Xu, and X. Shi (2011), Droplet nucleation: Physically-based parameterizations and comparative evaluation, *J. Adv. Model. Earth Syst.*, *3*, M10001, doi:10.1029/2011MS000074.

Ghan, S. J., X. Liu, R. C. Easter, R. Zaveri, P. J. Rasch, and J.-H. Yoon (2012), Toward a minimal representation of aerosols in climate models: Comparative decomposition of aerosol direct, semidirect, and indirect radiative forcing, *J. Clim.*, *25*, 6461–6476.

Giorgetta, A. M., et al. (2013), Climate and carbon cycle changes from 1850 to 2100 in MPI-ESM simulations for the Coupled Model Intercomparison Project phase 5, *J. Adv. Model. Earth Syst.*, *5*, 572–597, doi:10.1002/jame.20038.

Glotfelty, T., J. He, B. Gantt, and Y. Zhang (2013), Implementing a volatility basis set approach for simulation of secondary organic aerosol and its climatic impacts in CESM-CAM5, Abstract A31D-0107 presented at 2013 Fall Meeting, AGU, San Francisco, Calif., 9–13 Dec.

Guenther, A., T. Karl, P. Harley, C. Wiedinmyer, P. I. Palmer, and C. Geron (2006), Estimates of global terrestrial isoprene emissions using MEGAN (Model of Emissions of Gases and Aerosols from Nature), *Atmos. Chem. Phys.*, *6*, 3181–3210.

He, J., and Y. Zhang (2014), Improvement and further development in CESM/CAM5: Gas-phase chemistry and inorganic aerosol treatments, *Atmos. Chem. Phys.*, *14*, 9171–9200, doi:10.5194/acp-14-9171-2014.

Heald, C. L., et al. (2008), Predicted change in global secondary organic aerosol concentrations in response to future climate, emissions, and land use change, *J. Geophys. Res.*, *113*, D05211, doi:10.1029/2007JD009092.

Horowitz, L. W. (2006), Past, present, and future concentrations of tropospheric ozone and aerosols: Methodology, ozone evaluation, and sensitivity to aerosol wet removal, *J. Geophys. Res.*, *111*, D22211, doi:10.1029/2005JD006937.

Hudman, R. C., et al. (2007), Surface and lightning sources of nitrogen oxides over the United States: Magnitudes, chemical evolution, and outflow, *J. Geophys. Res.*, *112*, D12S05, doi:10.1029/2006JD007912.

Hurrell, J. W., et al. (2013), The Community Earth System Model: A framework for collaborative research, *Bull. Am. Meteorol. Soc.*, *94*, 1339–1360.

Iacono, M. J., J. S. Delamere, E. J. Mlawer, and S. A. Clough (2003), Evaluation of upper tropospheric water vapor in the NCAR Community Climate Model (CCM3) using modeled and observed HIRS radiances, *J. Geophys. Res.*, *108*(D2), 4037, doi:10.1029/2002JD002539.

Iacono, M. J., J. S. Delamere, E. J. Mlawer, M. W. Shephard, S. A. Clough, and W. D. Collins (2008), Radiative forcing by long-lived greenhouse gases: Calculations with the AER radiative transfer models, *J. Geophys. Res.*, *113*, D13103, doi:10.1029/2008JD009944.

Jimenez, J. L., et al. (2009), Evolution of organic aerosols in the atmosphere, *Science*, *326*, 1525–1529, doi:10.1126/science.1180353.

Karamchandani, P., Y. Zhang, S.-Y. Chen, and R. Balmori-Bronson (2012), Development of an extended chemical mechanism for global-through-urban applications, *Atmos. Pollut. Res.*, *3*, 1–24.

Kay, J. E., et al. (2012), Exposing global cloud biases in the Community Atmosphere Model (CAM) using satellite observations and their corresponding instrument simulators, *J. Clim.*, *25*, 5190–5207, doi:10.1175/JCLI-D-11-00469.1.

Keppel-Aleks, G., et al. (2013), Atmospheric carbon dioxide variability in the Community Earth System Model: Evaluation and transient dynamics during the twentieth and twenty-first centuries, *J. Clim.*, *26*, 4447–4475.

Koloutsou-Vakakis, S., M. J. Rood, A. Nenes, and C. Pilinis (1998), Modeling of aerosol properties related to direct climate forcing, *J. Geophys. Res.*, *103*(D14), 17,009–17,032, doi:10.1029/98JD00068.

Kumar, P., I. N. Sokolik, and A. Nenes (2009), Parameterization of cloud droplet formation for global and regional models: Including adsorption activation from insoluble CCN, *Atmos. Chem. Phys.*, *9*, 2517–2532, doi:10.5194/acp-9-2517-2009.

Lamarque, J.-F., J. T. Kiehl, P. G. Hess, W. D. Collins, L. K. Emmons, P. Ginoux, C. Luo, and X. X. Tie (2005), Response of a coupled chemistry-climate model to changes in aerosol emissions: Global impact on the hydrological cycle and the tropospheric burdens of OH, ozone, and NO_x, *J. Geophys. Res.*, *32*, L16809, doi:10.1029/2005GL023419.

Lamarque, J.-F., et al. (2012), CAM-chem: Description and evaluation of interactive atmospheric chemistry in CESM, *Geosci. Model Dev.*, *5*, 369–411, doi:10.5194/gmd-5-369-2012.

Lamarque, J. F., et al. (2013), The atmospheric chemistry and climate model intercomparison project: Overview and description of models, simulations and climate diagnostics, *Geosci. Model Dev.*, *6*, 179–206, doi:10.5194/gmd-6-179-2013.

Lance, S., et al. (2011), Cloud condensation nuclei as a modula-tor of ice processes in Arctic mixed-phase clouds, *Atmos. Chem. Phys.*, *11*, 8003–8015, doi:10.5194/acp-11-8003-2011.

Lane, T. E., N. M. Donahue, and S. N. Pandis (2008), Simulating secondary organic aerosol formation using the volatility basis-set approach in a chemical transport model, *Atmos. Environ.*, *42*(32), 7439–7451, doi:10.1016/j.atmosenv.2008.06.026.

Langmann, B., S. Varghese, E. Marmer, E. Vignati, J. Wilson, P. Stier, and C. O'Dowd (2008), Aerosol distribution over Europe: A model evaluation study with detailed aerosol microphysics, *Atmos. Chem. Phys.*, *8*, 1591–1607.

Lawrence, D. M., et al. (2011), Parameterization improvements and functional and structural advances in version 4 of the Community Land Model, *J. Adv. Model. Earth Syst.*, *3*, M03001, doi:10.1029/2011MS000045.

Levy, R. C., S. Mattoo, L. A. Munchak, L. A. Remer, A. M. Sayer, F. Patadia, and N. C. Hsu (2013), The Collection 6 MODIS aerosol products over land and ocean, *Atmos. Meas. Tech.*, *6*, 2989–3034, doi:10.5194/amt-6-2989-2013.

Lipscomb, W. H., J. G. Fyke, M. Vizcaino, W. J. Sacks, J. Wolfe, M. Vertenstein, A. Craig, E. Kluzek, and D. M. Lawrence (2013), Implementation and initial evaluation of the Glimmer Community Ice Sheet Model in the Community Earth System Model, *J. Clim.*, *26*, 7352–7371.

Liu, X., et al. (2012), Toward a minimal representation of aerosols in climate models: Description and evaluation in the Community Atmosphere Model CAM5, *Geosci. Model Dev.*, *5*, 709–739.

Martensson, E. M., E. D. Nilsson, G. deLeeuw, L. H. Cohen, and H. C. Hansson (2003), Laboratory simulations and parameterization of the primary marine aerosol production, *J. Geophys. Res.*, *108*(D9), 4297, doi:10.1029/2002JD002263.

Martin, G. M., et al. (2011), The HadGEM2 family of Met Office Unified Model climate configurations, *Geosci. Model Dev.*, *4*, 723–757, doi:10.5194/gmd-4-723-2011.

Merikanto, J., I. Napari, H. Vehkamaki, T. Anttila, and M. Kulmala (2007), New parameterization of sulfuric acid-ammonia-water ternary nucleation rates at tropospheric conditions, *J. Geophys. Res.*, *112*, D15207, doi:10.1029/2006JD007977.

Michoud, V., et al. (2012), Radical budget analysis in a suburban European site during the MEGAPOLI summer field campaign, *Atmos. Chem. Phys.*, *12*, 11,951–11,974, doi:10.5194/acp-12-11951-2012.

Mlawer, E. J., S. J. Taubman, P. D. Brown, M. J. Iacono, and S. A. Clough (1997), Radiative transfer for inhomogeneous atmospheres: RRTM, a validated correlated-k model for the longwave, *J. Geophys. Res.*, *102*(D14), 16,663–16,682.

Monier, E., J. R. Scott, A. P. Sokolov, C. E. Forest, and C. A. Schlosser (2013), An integrated assessment modeling framework for uncertainty studies in global and regional climate change: The MIT IGSM-CAM (version 1.0), *Geosci. Model Dev.*, *6*, 2063–2085.

Morrison, H., and A. Gettelman (2008), A new two-moment bulk stratiform cloud microphysics scheme in the community atmosphere model, version 3 (CAM3). Part I: Description and numerical tests, *J. Clim.*, *21*(15), 3642–3659.

Nakajima, T. Y., K. Suzuki, and G. L. Stephens (2010), Droplet growth in warm water clouds observed by the A-Train. Part I: Sensitivity analysis of the MODIS-derived cloud droplet sizes, *J. Atmos. Sci.*, *67*(6), 1884–1896, doi:10.1175/2009jas3280.1.

Neale, R. B., et al. (2012), Description of the NCAR Community Atmosphere Model (CAM5.0), *NCAR Tech. Note NCAR/TN-486+STR*, Natl. Cent. for Atmos. Res, Boulder, Colo.

Nenes, A., and J. H. Seinfeld (2003), Parameterization of cloud droplet formation in global climate models, *J. Geophys. Res.*, *108*(D14), 4415, doi:10.1029/2002JD002911.

O'Connor, F. M., et al. (2014), Evaluation of the new UKCA climate-composition model-Part 2: The Troposphere, *Geosci. Model Develop.*, *7*, 41–91, doi:10.5194/gmd-7-41-2014.

Park, S., and C. S. Bretherton (2009), The University of Washington shallow convection and moist turbulence schemes and their impact on climate simulations with the community atmosphere model, *J. Clim.*, *22*, 3449–3469.

Rausch, J., A. Heidinger, and R. Bennartz (2010), Regional assessment of microphysical properties of marine boundary layer cloud using the PATMOS-x dataset, *J. Geophys. Res.*, *115*, D23212, doi:10.1029/2010JD014468.

Reutter, P., H. Su, J. Trentmann, M. Simmel, D. Rose, S. S. Gunthe, H. Wernli, M. O. Andreae, and U. Pöschl (2009), Aerosol- and updraft-limited regimes of cloud droplet formation: Influence of particle number, size and hygroscopicity on the activation of cloud condensation nuclei (CCN), *Atmos. Chem. Phys.*, *9*, 7067–7080, doi:10.5194/acp-9-7067-2009.

Seethala, C., and Á. Horvath (2010), Global assessment of AMSR-E and MODIS cloud liquid water path retrievals in warm oceanic clouds, *J. Geophys. Res.*, *115*, D13202, doi:10.1029/2009JD012662.

Smith, S. R., D. M. Legler, and K. V. Verzone (2001), Quantifying uncertainties in NCEP reanalyses using high-quality research vessel observations, *J. Clim.*, *14*, 4062–4072, doi:10.1175/1520-0442(2001)014<4062:QUINRU>2.0.CO;2.

Sokolov, A. P., et al. (2005), The MIT Integrated Global System Model (IGSM) Version 2: Model description and baseline evaluation, *MIT JPSPGC Rep. 124*, 40 p., MIT Joint Program on the Sci. and Policy of Global Change, Cambridge, Mass.

Sorjamaa, R., and A. Laaksonen (2007), The effect of H_2O adsorption on cloud drop activation of insoluble particles: A theoretical framework, *Atmos. Chem. Phys.*, *7*, 6175–6180.

Stevens, B., et al. (2013), Atmospheric component of the MPI-M Earth System Model: ECHAM6, *J. Adv. Model. Earth Syst.*, *5*, 146–172, doi:10.1002/jame.20015.

Taylor, K. E. (2001), Summarizing multiple aspects of model performance in a single diagram, *J. Geophys. Res.*, *106*(D7), 7183–7192.

Textor, C., et al. (2006), Analysis and quantification of the diversities of aerosol life cycles within AeroCom, *Atmos. Chem. Phys.*, *6*, 1777–1813, doi:10.5194/acp-6-1777-2006.

Tsigaridis, K., M. Krol, F. J. Dentener, Y. Balkanski, J. Lathiere, S. Metzger, D. A. Hauglustaine, and M. Kanakidou (2006), Change in global aerosol composition since preindustrial times, *Atmos. Chem. Phys.*, *6*, 5143–5162.

Vehkamaki, H., M. Kulmala, I. Napari, K. E. J. Lehtinen, C. Timmreck, M. Noppel, and A. Laaksonen (2002), An improved parameterization for sulfuric acid-water nucleation rates for tropospheric and stratospheric conditions, *J. Geophys. Res.*, *107*(D22), 4622, doi:10.1029/2002JD002184.

Wang, M., and J. E. Penner (2009), Aerosol indirect forcing in a global model with particle nucleation, *Atmos. Chem. Phys.*, *9*, 239–260.

Williams, J. E., M. P. Scheele, P. F. J. van Velthoven, J.-P. Cammas, V. Thouret, C. Galy-Lacaux, and A. Volz-Thomas (2009), The influence of biogenic emissions from Africa on tropical tropospheric ozone during 2006: A global modeling study, *Atmos. Chem. Phys.*, *9*, 5729–5749.

Xie, S., X. Liu, C. Zhao, and Y. Zhang (2013), Sensitivity of CAM5-simulated arctic clouds and radiation to ice nucleation parameterization, *J. Clim.*, *26*, 5981–5999, doi:10.1175/JCLI-D-12-00517.1.

Yu, F. (2010), Ion-mediated nucleation in the atmosphere: Key controlling parameters, implications, and look-up table, *J. Geophys. Res.*, *115*, D03206, doi:10.1029/2009JD012630.

Zender, C. S., H. Bian, and D. Newman (2003), The mineral dust entrainment and deposition (DEAD) model: Description and 1990s dust climatology, *J. Geophys. Res.*, *108*(D14), 4416, doi:10.1029/2002JD002775.

Zhang, G. J., and N. A. McFarlane (1995), Sensitivity of climate simulations to the parameterization of cumulus convection in the Canadian Climate Centre general circulation model, *Atmos. Ocean*, *33*, 407–446.

Zhang, Q., et al. (2007), NO_x emission trends for China, 1995–2004: The view from the ground and the view from space, *J. Geophys. Res.*, *112*, D22306, doi:10.1029/2007JD008684.

Zhang, Q., et al. (2009), Asian emissions in 2006 for the NASA INTEX-B mission, *Atmos. Chem. Phys.*, *9*, 5131–5153, doi:10.5194/acp-9-5131-2009.

Zhang, Y., P. Karamchandani, T. Glotfelty, D. G. Street, G. Grell, A. Nenes, F. Yu, and R. Bennartz (2012), Development and initial application of the global-through-urban weather research and forecasting model with chemistry (GU-WRF/Chem), *J. Geophys. Res.*, *117*, D20206, doi:10.1029/2012JD017966.

Zhang, Z., and S. Platnick (2011), An assessment of differences between cloud effective particle radius retrievals for marine water clouds from three MODIS spectral bands, *J. Geophys. Res.*, *116*, D20215, doi:10.1029/2011JD016216.